Numerical Simulation of Hydrothermal Salt Separation Process and Analysis and Cost Estimating of Shipboard Liquid Waste Disposal

by

Andrew Robert Hunt

B.S. Systems Engineering
United States Naval Academy, 1997

Submitted to the Department of Mechanical Engineering in Partial Fulfillment of the Requirements for the Degrees of

Naval Engineer

and

Master of Science in Mechanical Engineering

at the
Massachusetts Institute of Technology
June 2007

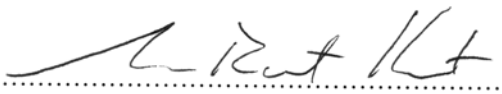

Signature of Author: .....
Department of Mechanical Engineering
May 18, 2007

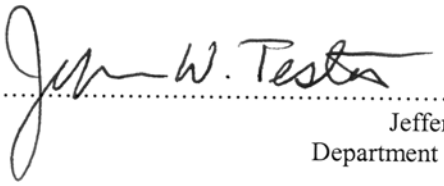

Certified by: .....
Jefferson W. Tester, Professor
Department of Chemical Engineering
Thesis Supervisor

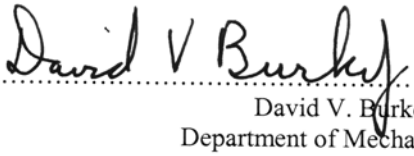

Certified by: .....
David V. Burke, Senior Lecturer
Department of Mechanical Engineering
Thesis Reader

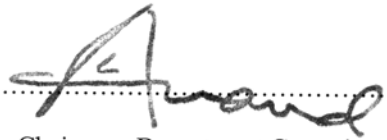

Accepted by: .....
Lallit Anand
Chairman, Department Committee on Graduate Students

REPORT DOCUMENTATION PAGE

Form Approved
OMB No. 0704-0188

1. REPORT DATE *(DD-MM-YYYY)*	2. REPORT TYPE	3. DATES COVERED *(From - To)*
XX-06-2007	Master's Thesis	JAN-JUN 2007

4. TITLE AND SUBTITLE

Numerical Simulation of Hydrothermal Salt Separation Process and Analysis and Cost Estimating of Shipboard Liquid Waste Disposal

5a. CONTRACT NUMBER
N62271-97-G-0026

5b. GRANT NUMBER

5c. PROGRAM ELEMENT NUMBER

6. AUTHOR(S)
Andrew R. Hunt

5d. PROJECT NUMBER

5e. TASK NUMBER

5f. WORK UNIT NUMBER

7. PERFORMING ORGANIZATION NAME(S) AND ADDRESS(ES)
Massachusetts Institute of Technology

8. PERFORMING ORGANIZATION REPORT NUMBER

9. SPONSORING / MONITORING AGENCY NAME(S) AND ADDRESS(ES)
Naval Postgraduate School
Monterey, Ca 93943

10. SPONSOR/MONITOR'S ACRONYM(S)
NPS

11. SPONSOR/MONITOR'S REPORT NUMBER(S)

12. DISTRIBUTION / AVAILABILITY STATEMENT
1. DISTRIBUTI9ON STATEMENT A. Approved for public release; distribution is unlimited.

13. SUPPLEMENTARY NOTES

14. ABSTRACT

Due to environmental regulations, waste water disposal for US Navy ships has become a requirement which impacts both operations and the US Navy's budget. In 2006, the cost for waste water disposal Navy-wide was 54 million dollars. There are many advanced waste water treatment technologies in the research and development stage at academic institutions, private corporations, and government labs. Additionally, considerable progress has been made in installing and operating unique waste water treatment systems onboard merchant and commercial vessels, showing that waste water treatment technologies are near the maturity level required for installation on US Navy ships. Installation and operations costs can be estimated from data collected from merchant ships, but the accompanying life cycle liquid disposal costs savings can be difficult to estimate. A cost estimator is presented which allows variations in ship's operational schedule and aids in determining the total life cycle savings, and the time for return on investment, when waste destruction technologies are installed in a class of ship. Additionally, the properties of one waste water destruction medium, supercritical water, are reviewed and its use in efficient and environmentally safe chemical processes are discussed. In particular, supercritical water is the medium of choice for the performance of a biomass to synthetic natural gas conversion process. The supercritical water is utilized to aid in a vital salt separation process which allows for efficient 4 hydrothermal gasification. Numerical simulations of the salt separation process are completed which help in understanding the flow properties. The results will aid in yielding an optimized salt separation process, improving the efficiency and viability of the conversion process.

15. SUBJECT TERMS

16. SECURITY CLASSIFICATION OF:			17. LIMITATION OF ABSTRACT	18. NUMBER OF PAGES	19a. NAME OF RESPONSIBLE PERSON
a. REPORT	b. ABSTRACT	c. THIS PAGE			Sean Tibbitts, Educational Technician
			UU	95	19b. TELEPHONE NUMBER *(include area code)* (831) 656-2319 civins@nps.edu

Standard Form 298 (Rev. 8-98)
Prescribed by ANSI Std. Z39.18

Page Intentionally Left Blank

Numerical Simulation of Hydrothermal Salt Separation Process and Analysis and Cost Estimating of Shipboard Liquid Waste Disposal

by

Andrew Robert Hunt

Submitted to the Department of Mechanical Engineering
On May 18, 2007
in Partial Fulfillment of the Requirements for the Degrees of

Naval Engineer
and
Master of Science in Mechanical Engineering

Abstract

Due to environmental regulations, waste water disposal for US Navy ships has become a requirement which impacts both operations and the US Navy's budget. In 2006, the cost for waste water disposal Navy-wide was 54 million dollars. There are many advanced waste water treatment technologies in the research and development stage at academic institutions, private corporations, and government labs. Additionally, considerable progress has been made in installing and operating unique waste water treatment systems onboard merchant and commercial vessels, showing that waste water treatment technologies are near the maturity level required for installation on US Navy ships. Installation and operations costs can be estimated from data collected from merchant ships, but the accompanying life cycle liquid disposal costs savings can be difficult to estimate. A cost estimator is presented which allows variations in ship's operational schedule and aids in determining the total life cycle savings, and the time for return on investment, when waste destruction technologies are installed in a class of ship.

Additionally, the properties of one waste water destruction medium, supercritical water, are reviewed and its use in efficient and environmentally safe chemical processes are discussed. In particular, supercritical water is the medium of choice for the performance of a biomass to synthetic natural gas conversion process. The supercritical water is utilized to aid in a vital salt separation process which allows for efficient

hydrothermal gasification. Numerical simulations of the salt separation process are completed which help in understanding the flow properties. The results will aid in yielding an optimized salt separation process, improving the efficiency and viability of the conversion process.

Thesis Supervisor: Jefferson W. Tester
Title: Professor of Chemical Engineering

Thesis Reader: David V. Burke
Title: Senior Lecturer Department of Mechanical Engineering

Table of Contents

List of Tables

List of Figures

Acknowledgements

I would like to thank Professor Jeff Tester, my thesis adviser, for supporting my research efforts by providing both technical advice and constant encouragement. In addition to providing thesis advisement, he gave me the opportunity to work with intelligent, hard working people in a fascinating field. The items I was exposed to outside of my research area will serve me in my future endeavors.

Thanks to Dr. Fredi Vogel from the Paul Scherrer Institut for providing invaluable technical guidance.

Thanks to Dr. David Burke for igniting my interest in Thermodynamics and setting me on an initial course towards my area of research.

Special thanks to all members of the Tester Research Group who seamlessly welcomed me into the group and patiently answered my endless questions. Andy Peterson, Chad Augustine, Scott Papp, Rocco Ciccolino - I couldn't have completed my research without your help.

Thanks to my family, my wife Ronny and my mom and dad, for supporting me through the ups and downs.

1. Introduction

Chemical Engineering research in industry and academia has long searched for unique processes which make desired reactions occur more efficiently. The goals of these research efforts are multiple and include reducing necessary caustic catalysts and solvents, reducing reaction times, reducing harmful byproducts, or reducing process steps. Research, as with many things, is driven by economic incentives. Fortunately, environmental incentives exist too. A process which needs less catalyst or solvent uses fewer materials and has the potential for lower cost. A process which yields benign byproducts will have less negative impact on the environment and also have lower clean-up costs. A more efficient reaction process will yield more products in less time. All these improvements impact the cost of business, both economic and environmental.

The US Navy has been looking to these unique physical, chemical, and biological processes as a way to reduce liquid waste disposal costs and improve compliance with environmental regulations. There are a variety of different liquid waste disposal processes now in use in commercial vessels, and their suitability for installation on US Navy ships must be considered. The decision to install a waste water treatment system must consider the environmental, operational, and economic impact for the US Navy and its ships, and the technological state of the waste disposal process. An estimate of liquid waste disposal life cycle cost is useful when determining if a return on investment does occur. A review of current technologies and a cost estimator are presented in Chapter 6.

In addition to technologically mature chemical processes, and in light of today's energy issues, there are many academic and private research groups which are investigating methods to produce energy from waste. One particular process being investigated is a hydrothermal process which converts biomass feedstock (in particular, a solution of water and cow manure) into a useable energy carrier. Work is currently in initial stages, and research into process optimization and scale up is essential to the long term success of the process. The research contained in Chapters 2 through 5 cover numerical simulations for a portion of the process. The goal is to gain a better understanding of the fluid flow properties in the bench scale reactor and apply lessons learned when increasing to an industrial size process.

1.1 Thesis and general approach

The initial portions of the research will focus on the numerical simulations for the salt separation process that is in practice at the Paul Scherrer Institut in Switzerland. The approach is to model the physical process that was first implemented in SALSAN and then improved upon in Konti-2. Computer modeling of the salt separation vessel is useful for understanding how the aqueous solution behaves as the temperature of the fluid increases from sub-critical to super-critical. Models of various dimensions, flow rates, and temperatures are developed, enabling optimization of the process while minimizing physical experiments. SALSAN is the stand along, bench scale salt separation vessel constructed and tested at the Paul Scherrer Institut (PSI) in Switzerland. It will be described in detail in Chapter 4. Konti-2 is the Supercritical Water Gasification bench scale model that has also been constructed at PSI. A part of Konti-2 is a salt separation vessel with similar, but not exact, characteristics to SALSAN. Its operation parameters will be described in Chapter 5. Although numerical simulations were performed for the salt separation vessels in both SALSAN and Konti-2, only the results from the SALSAN simulations are presented here.

In Chapter 6, a high level review of existing waste destruction technologies will be conducted. This review will include analysis of current shipboard liquid waste treatment and destruction processes, comparison of which processes may be most viable for US Navy use, and a cost estimator which allows for comparison of liquid waste disposal with potential installation and operations cost. The intent of the cost analysis is to show that, in addition to the environmental benefits of effectively treating shipboard waste using a range of available methods, there are also economic benefits which can be realized over the lifetime of a ship.

2.1 Salt Separation as Part of the Biomass to Methane Process

Chemical and physical processes utilizing the unique properties of supercritical fluids have been investigated as possible means to improve a variety of processes: supercritical water in steam Rankine cycles (fossil-fuel powered plants), supercritical carbon dioxide and supercritical water in advanced nuclear power plants, and oxidation in supercritical water for use in destroying toxic military wastes and chemical wastes (i.e. stockpiled chemical warfare agents and industrial agents) have all been studied and modeled. Beyond these processes, and in light of recent energy initiatives, there are experiments in progress which hope to produce methane from a variety of biomass feedstocks via a catalytic conversion process. Differing from Supercritical Water Oxidation, where organic waste is oxidized, experiments have shown that it is possible to separate useful compounds (methane, for example) from organic solutions. These solutions, containing primarily organic matter, salts, and water, require specific processing in order to extract useful compounds. Specifically, it is necessary to extract salts from the solution prior to the catalytic conversion process, as salts will poison the catalyst, lowering activity and adversely affecting yields and the continuity of operations. Separating the salts is not a simple process, and the impact of salt accumulation and corrosion during the separation function can greatly affect process efficiency and, in extreme cases, process viability. Studies to understand and control the salt separation process are essential to minimizing the impact of the corrosion and salt accumulation.

A proposed method for salt separation is to simply separate precipitated salts from the supercritical biomass solution in a reverse-flow, brine pool reactor vessel. As desired, this process allows separation of salt from solution prior to the gasification and methane extraction process. By separating salts, the hope is to reduce unsatisfactory salt accumulation and allow the gasification to occur as a constant feed process versus a single batch process. The removal of the salt will allow the process to achieve catalytic stability in the following processing steps. As an added bonus, the removed salts can be recovered and used as fertilizer. The entire process of waste to fuel will improve energy sustainability in a number of ways: 1) through collection of the biomass, a reduction in

the amount of methane, a greenhouse gas, which is emitted into the atmosphere 2) production of a familiar fuel which can is already used in many energy production systems 3) through the collection of the salts, a reduction in the amount of natural gas and energy necessary to produce fertilizers.

The presented research focuses on the numerical modeling of salt separation processes in supercritical water in a MODAR-type reactor vessel using ANSYS CFX Computational Fluid Dynamic (CFD) software. The goal is to demonstrate the feasibility of using ANSYS CFX CFD software for modeling salt separation. If successful, such a model would be valuable in optimizing the salt separation process at reduced experimental cost. With the use of simulation software, reactor parameters (flow rate, temperatures, pressure, inlet location, etc) can be varied and results compared to determine which combination yields the most favorable results. Specifically, the axial location of the flow reversal will aid in determining where salts will precipitate out of the water-organic waste solution and give indications of how to deal with salt build-up and corrosion. As a starting point, the initial work presented here will model the flow path of pure water.

2.2 Background and motivation

Supercritical Water Oxidation (SCWO) is a hydrothermal oxidation process in which organic wastes are destroyed in an aqueous solution without harmful byproducts. For example, an H-C-N-S-P hydrocarbon compound will be fully mineralized to CO_2, H_20, and N_2, with SO_4 and PO4 that can be neutralized with NaOH to form soluble salts. SCWO, characterized by operating temperatures and pressures within the reactor vessel above the critical point of water (T_c = 374 °C, P_c = 220 bar), has been studied over the past 25 years. The goal of this research is to achieve industrial size reactors which can continuously and efficiently perform hydrothermal processes, whether that be oxidation of organic wastes or separation inorganic salts using a harmful byproduct-free process.

Supercritical water oxidation reactor systems come in many configurations, creating unique reactor designs which allow the SCWO reactor to have a higher operational availability for a particular application [23]. There have been efforts by private companies and government laboratories to produce advanced reaction vessel devices and operating schemes in order to reduce the amount of corrosion and/or salt build-up that is inherent in the SCWO process, and thereby make their systems usable for continuous flow, versus "batch" operations. As covered by Marrone et al. (2003), a variety of methods have been developed to control salt precipitation and solid build-up in the reaction vessel. Generally, separation methods can be divided into two different categories: those with unique reactor or system design, and those that use special operating methods. As examples of unique design, MODAR has developed a reverse flow, tank reactor with a brine pool, and Foster Wheeler has developed a transpiring wall reactor. As examples of salt removal specific methods, General Atomics has developed a reactor which uses reactor flushing, and MODEC has developed a mechanical brushing mechanism for their reactor.

2.3 Bio-fuels motivation

Another application for hydrothermal treatment is a catalytic reaction process where a variety of biomass feedstocks, including organic waste, sludges, and agriculture and forestry wastes, can be processed in supercritical water to produce useful energy and fuel byproducts, including a synthetic natural gas which can be used in traditional methane combustion processes. Supercritical water, which is the medium for this catalytic conversion process to ensure acceptable reaction rates and conversion, is also used to separate salts from the biomass/water solution. Supercritical water is utilized because of the salt solubility in water changes rapidly at the critical point. Many salts, which are soluble in water at sub-critical temperatures, will precipitate out of solution when the heated from sub-critical to super-critical temperatures. In principle, the salt separation process is a simple physical process which requires only heat addition.

The benefits of the salt separation process in the hydrothermal biomass gasification process are twofold. First, salts which can interfere with the catalytic conversion process of the organic compounds are removed from the solution prior to contacting the catalyst. Second, the separated salts can be collected and re-used as a nitrogen-rich fertilizer. This useful byproduct lowers environmental impacts by reducing natural gas needed for generating hydrogen used in ammonia fertilizer manufacturing, thereby reducing energy consumption.

2.4 Study Specifics

Numerous studies have been performed which investigate heat transfer ([20], [36]), numerical models ([17], [26], [29]), and other general properties of fluid flow involving supercritical fluids [5]. Of the 15 numerical simulation papers reviewed in preparation for this study, all but one are steady state simulations in two dimensions. Two dimensional, axi-symmetric simulations have been performed in favor of the more computational intensive and complex three dimensional simulations. In the case of SALSAN and Konti-2 salt separation vessels, with an off axis flow port (exit port), symmetry (geometric, flow, or otherwise) does not exist and therefore two dimensional simulations do not properly capture the complexity of the flow. For this reason, three dimensional simulations are necessary.

The inclusion of a third dimension in the numerical simulation creates a problem of higher complexity. Although governing equations for the flow are the same, the addition of the third dimension creates a much larger array for manipulation and solving of the discretized equations. Also, applying techniques of linear algebra (the preferred implementation method in numerical simulations) becomes more computationally intensive in three dimensions.

2.5 Criteria for success.

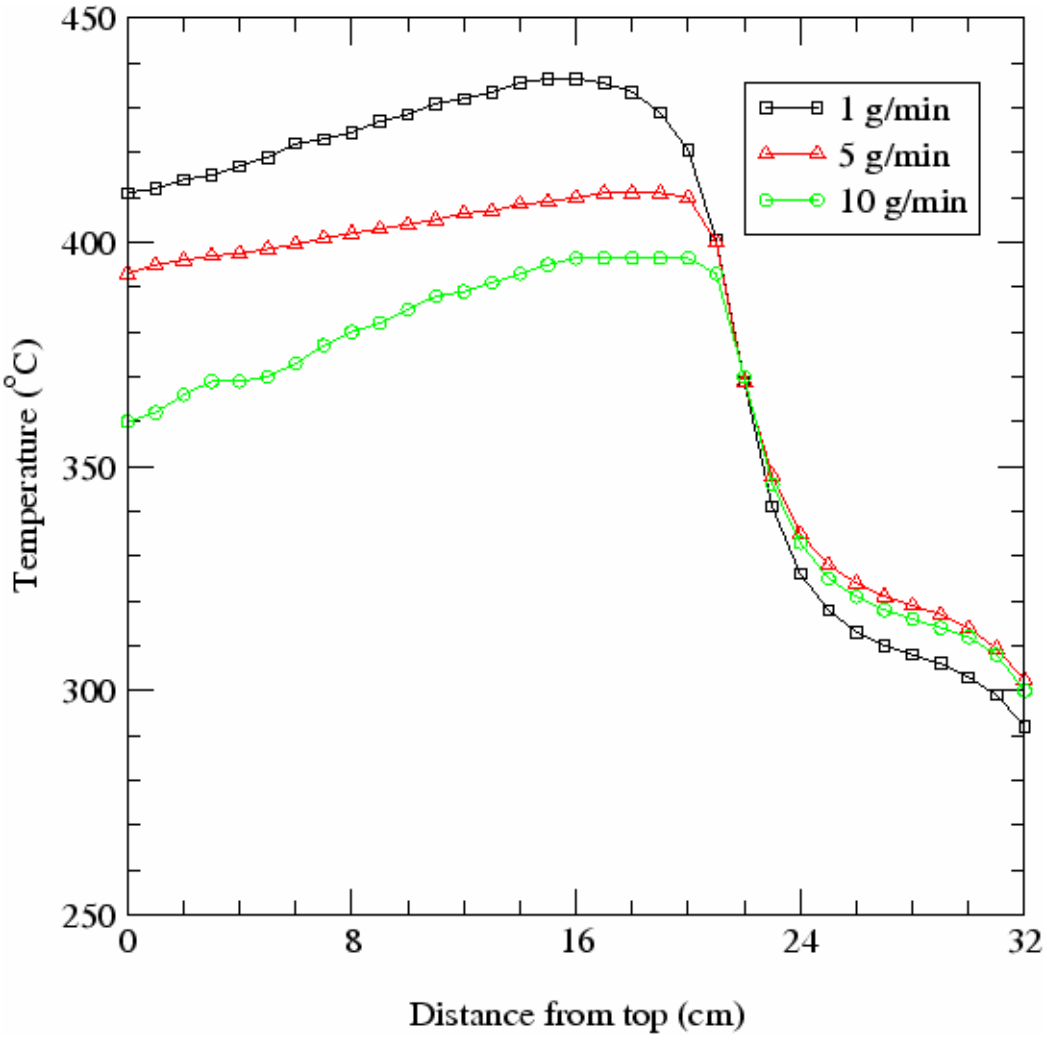

Figure 1 Experimental Results from SALSAN Salt Separation Vessel [27]

Figure 1 shows temperature readings taken from experiments in SALSAN, a model separation vessel, performed at PSI. Results from numerical analysis will be compared to the experimental data points for the three different inlet flow rates. Lessons learned while conducting the bench scale simulations will be applied in further studies and the optimization of the scale-up process.

3. Exploring the Properties of Sub- and Supercritical Water

Chemical and physical processes involving supercritical fluids behave in unique ways due to large variations in fluid physical properties at the psuedo-critical point. At pressures near the critical value of 220 bar, the density, thermal conductivity, enthalpy, and viscosity all change rapidly as the temperature passes through the critical point.

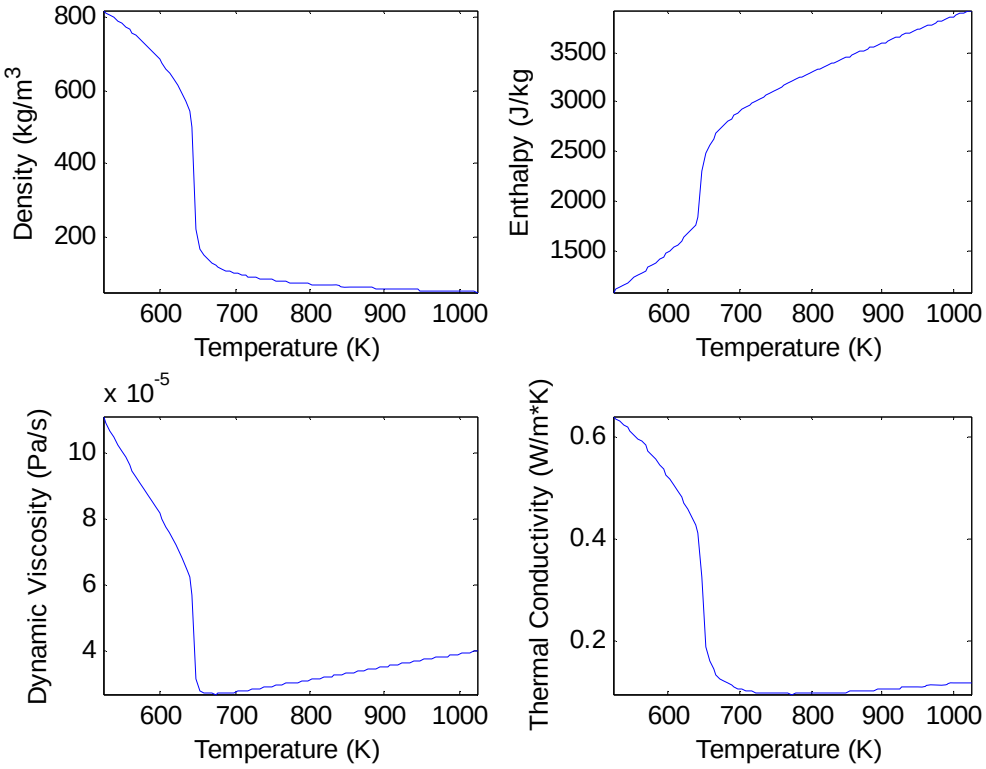

Figure 2

Figure 2.a shows relevant fluid properties for pure water at the critical pressure, 221 bar. Note the rapid change in all property values as temperature reaches the critical temperature of 647 degrees K. Values are from the industrial standard IAPWS-IF97.

These unique changes in thermo-physical properties can be exploited in a number of different physical processes. At and above water's critical point of 374 degrees Celsius and 221 bar, the liquid to gas co-existence (or the liquid-vapor equilibrium line) ceases to exist and the fluid simply experiences physical property changes similar to that of a dense

fluid without traditional phase transition. In conjunction with these physical phenomena, the fluid properties (enthalpy, viscosity, density, thermal conductivity, dielectric constant, etc.) rapidly change over small temperature and pressure variations near the critical point, thereby affecting water's solvation power with other compounds. These rapid changes can be exploited in physical processes, for example in a supercritical steam plant or in a Supercritical Water Oxidation (SCWO) waste destruction system.

3.1 Finite Element Model

A finite element model provides a representation of a physical system with the use of mathematical equations that describe momentum, energy, and mass transport based on constitutive representations. For a three dimensional numerical model, three specific sections or regions were selected to represent the portions of the experimental set-up. In the case of both SALSAN and Konti-2 vessels, there are three, 3-D volumes of interest. Each volume must be modeled using known equations that adequately represent the physical system. These three volumes are the injection needle (made of solid stainless steel), the vessel reaction zone (cylindrical shaped fluid zone), and the actual reaction vessel itself (12 mm thick Zircaloy, in the case of SALSAN). The equations of conservation of mass, conservation of momentum, and conservation of energy are applied to each volume and to the system as a whole. For the two solids (needle injection tube and Zircaloy vessel wall), heat conduction in the body and heat transfer to the fluid are modeled. In the fluid region, the solution is more complicated, as flow properties (velocity vectors and pressure) must be evaluated in addition to heat transfer and conduction. For the entire system, mass and energy balances are required in order to achieve a solution.

The desired solution for this fluid flow problem is the evaluation of the velocity, temperature, and pressure of the fluid at each point in the reactor. In order to achieve this goal, the three volumes of interest will be finitely discretized into many individual control volumes. Many in this case means O(10^6) control volumes. For each control volume, or finite element, the governing equations are solved and mean properties calculated.

Also, for each individual control volume, an equation residual is calculated. This equation residual is the difference between the solved values for the left hand side and right hand side of each governing equation applied at the control volume. This residual value gives an indication of the precision of the mathematical model. (Residual values and their analysis are discussed further in Chapter 5.) In order to solve the governing equations over a large number of control volumes, computer programs are written which can accurately and iteratively solve very large number of simplified equations. The process of manipulating the continuous governing equations to yield the simplified discrete equations, and the resulting solution accuracy of these manipulations, has been studied by finite element theorists for decades. With the advent of computationally powerful computers, these studies have become much more popular among researchers.

3.1.1 Governing Equations

The equations solved over each finite element control volume are the continuity equation, linear momentum equation, and an energy conservation equation. Each of these equations can be written in many different forms, depending on the particular situation. For fluid flow, it is important to use equations which match the physical realities. In other words, using a continuity or momentum equation which assumes incompressible flow will yield incorrect results if the actual physical system is a compressible flow case. Similarly, if the energy equation neglects mechanical energy, one must be sure that mechanical energy is not important to the physical problem of interest. The continuous continuity, momentum, and energy equations for a compressible Newtonian fluid, involving kinetic and thermal energy, are described below.

Due to the temperature variation and high pressure operation of both the SALSAN and Konti-2 salt separation vessels, the fluid flow characteristics will be greatly impacted by spatial and temporal variations in fluid property - particularly the fluid density. This type of flow, where changes in fluid density largely impact the flow characteristics, is considered to be compressible flow. The standard Navier-Stokes equation governing fluid flow is normally derived and presented with the assumption of

incompressible flow, where density changes in the fluid are not present, do not impact the total flow properties, or change as a function of pressure. It is important to consider the additional terms that are captured in the Navier-Stokes equations which do not assume incompressibility. Although it may be tempting to simply include the complete compressible flow Navier-Stokes equations ((without consideration of "special cases", i.e. incompressible flow) as a starting point, a complete derivation is helpful and may yield better understanding of the discretized equations and the turbulence models used to supplement the Reynolds Averaged Navier-Stokes (RANS) equation.

For any control volume, the fundamental conservation laws can be derived by applying the Reynold's Transport Theorem (RTT), which is a simple statement of the rate of change of any extensive property of a system.

Accumulation of X in V	=	Rate of X created in V + X flowing into V through S - X flowing out of V through S	(1)

where X = any extensive property
V = the control volume
S = the surface of the control volume

Continuity and Momentum Conservation

From the RTT, the integral balance equations for the fundamental conservation laws can be created. For fluid mechanics, mass and momentum can be implemented into the RTT to yield the continuity equation and linear momentum equation.

$$d/dt \int_V \rho \, dV + \int_S \rho \, \mathbf{u} \bullet \mathbf{n} \, dS = 0$$

Continuity Equation (2)

$$d/dt \int_V \rho \, \mathbf{u} \, dV + \int_S \rho \, \mathbf{u} \, \mathbf{u} \bullet \mathbf{n} \, dS = \int_V \rho \, g \, dV + \int_S -P \bullet \mathbf{n} \, dS$$

Linear Momentum

Equation (inviscid) (3)

ρ = fluid density (scalar)
u = fluid velocity (vector)
n = the outward facing normal (vector)
g = gravitational constant
P = pressure
t = time
V = the Volume of interest
S = the Surface of the Volume of interest

In the above equations, volume integrals relate to source/accumulation terms and surface integrals are the summation of fluxes through the surface.

Applying the divergence theorem to transform the surface integrals to volume integrals, they become:

$$\int_V d/dt \, \rho \, dV + \int_S \nabla \bullet (\rho \, \mathbf{u}) \, dV = 0$$

(2a)

$$\int_V d/dt \, (\rho \, \mathbf{u}) \, dV + \int_S \nabla \bullet (\rho \, \mathbf{u} \, \mathbf{u}) \, dS = \int_V \rho \, g \, dV - \int_S \nabla P \, dV$$

(3a)

And since the volume V is any arbitrary volume, the integrals can be removed, leaving the differential equation form of the continuity and linear momentum equations:

$$d/dt \, \rho + \nabla \bullet (\rho \, \mathbf{u}) = \mathbf{0}$$

(2b)

$$d/dt \, (\rho \, \mathbf{u}) + \rho \, \mathbf{u} \, \nabla \bullet \mathbf{u} + \mathbf{u} \bullet \nabla (\rho \mathbf{u}) = \rho g - \nabla P$$

(3c)

Further reduction, using the definition of the material derivative and doing some rearrangements and grouping of terms

$$D/Dt = d/dt + \underline{u}\bullet\nabla$$

Material Derivative (4)

yields the continuity and linear momentum equation for compressible fluid flow.

$$D\rho/Dt + \rho\nabla\bullet\mathbf{u} = 0$$

Continuity Equation (5)

$$\rho\, D\mathbf{u}/Dt = -\nabla P + \rho g$$

Linear Momentum Equation (6)

In the derivation of these equations, there are no assumptions made about the material or flow itself, therefore the equations apply to all fluid flows. At this point, an important difference between the compressible and incompressible balance equations should be emphasized. The incompressible version of the continuity equation, where the material derivative taken with respect to density is zero, is:

$$\nabla\bullet\mathbf{u} = 0$$

Incompressible Continuity Equation (5a)

So for equations (5) and (6), there are four equations (continuity and Euler in three dimensions) with five unknowns: three orthogonal velocity components (u, v, w), density (ρ), and pressure(P). For the incompressible case, there are four equations but only four unknowns (u,v,w, and P). Therefore, in the compressible case, equations (5a) and (6) are sufficient to solve for the fluid flow. They are not, sufficient, however for solving for the fluid flow in the compressible case.

Equation of Motion for Fluid Particle: For better understanding of ideas presented later in this paper, it is worth looking at the equation of motion for one individual fluid

particle. If one considers an infinitesimally small fluid particle, with the associated stresses on each side (as shown in Figure 3),

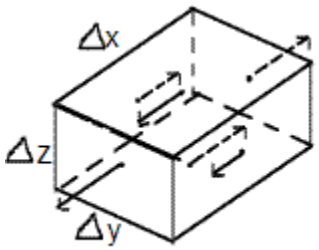

Figure 3 Fluid Particle with Stresses on Each Face

The equation of motion in the x direction, which relates the mass times the acceleration to the surface forces acting on the body, can be written:

$$\rho \Delta x \Delta y \Delta z \, Dv_x/Dt = (\partial \tau_{xx}/\partial x + \partial \tau_{xy}/\partial y + \partial \tau_{xz}/\partial z) \, \Delta x \Delta y \Delta z + \rho \Delta x \Delta y \Delta z \, F_x \quad (6)$$

F_x = body force in the x direction (per unit mass)

Dividing by the volume yields the equation of motion for the particle fluid.

$$\rho Dv_x/Dt = (\partial \tau_{xx}/\partial x + \partial \tau_{xy}/\partial y + \partial \tau_{xz}/\partial z) + \rho F_x \quad (6a)$$

The stress terms for the fluid particle can be related to the rate of strain for the fluid particle when using a newtonian fluid assumption. Texts present the stress-strain relationship derivation in various manners [25, p. 60 - 62], and results are presented here with brief discussion. First, it is recognized that if no fluid motion is present, there does exist the pressure stress within the fluid which equilibrates the forces acting on a fluid particle. This fluid stress can be written:

$\tau_{ij} = -P \, \delta_{ij}$, where δ_{ij} is the Kroenecker delta function.

When relative motion between the fluid particles is present, then viscous stresses in addition to the pressure stress will be present. These viscous stresses can be written as $\tau_{ij} = \mu (\partial u_i/\partial x_j + \partial u_j/\partial x_i)$

Combining the pressure stress and the viscous shear stress terms, the total stress tensor is

$$\tau_{ij} = -P\,\delta_{ij} + \mu (\partial u_i/\partial x_j + \partial u_j/\partial x_i) \tag{7}$$

The term τ_{ij} is the stress tensor and can be substituted into the momentum equation for certain unknown terms. Substituting the stress tensor from (7) into equation (6) yielding the momentum equation

$$\partial(\rho \mathbf{u})/\partial t + \mathbf{u}\nabla\bullet\rho\mathbf{u} = \nabla\bullet\tau_{ij} + F_{ext} \tag{8}$$

τ_{ij} encapsulates both the pressure force and the internal forces, represented by ρg in equation (6).

Energy Equation: The energy equation can be derived from the entropy and enthalpy balance integrals in the same way that the continuity and momentum equations were derived. Simplification of the energy equation can be somewhat more difficult, as energy terms can come from mechanical, potential, magnetic, kinetic, friction, or thermal sources.

In the case of the salt separation vessel, the relevant energy types include internal and kinetic. The energy equation for the fluid flow in the salt separator can be written, neglecting potential energy effects:

$$\partial(\rho h_{total})/\partial t - \partial p/\partial t + \nabla\bullet(\rho\ \mathbf{u}\ h_{total}) = \nabla\bullet(\lambda\nabla T) + \nabla\bullet(\mathbf{u}\bullet\tau) + E_{source} \tag{9}$$

$h_{total} = h + .5*\mathbf{u}\text{^}2$, or total specific methalpy
h= specific enthalpy
λ = thermal conductivity of the fluid
E_{source} = an energy source

ρ = the fluid density
t = the time
T = the temperature
τ = the stress tensor in Equation (7)
p = Pressure

The third term on the right hand side of equation (9) containing the stress tensor is due to viscous dissipation, and represents the addition of frictional heat resulting from fluid particle interactions. Recalling that the stress tensor includes the multiplication of the dynamic viscosity with the rate of strain of the fluid particle adds to the understanding of the viscous dissipation nomenclature.

In total, for the three governing equations, there are seven unknowns: the temperature, pressure, density, velocities in three directions (u, v, w), and enthalpy. In order to find a solution, a constitutive property model or Equation of State, which relates the density of the fluid as a function of both temperature and pressure, is needed:

$\rho = \rho(p,T)$

Various mathematical formulations of an Equation of State (EOS) can be used to represent density as a function of temperature and pressure that are sufficiently accurate. For example, the ideal gas EOS ($\rho = RT/p$) when appropriate, or the Redlich Kwong cubic EOS can be used for real gases. These equations are valid only for certain conditions (ranges of temperature and pressure/density) so it is important to validate the EOS with known values in the region of interest. A second important property is enthalpy as a function of temperature and pressure. Various functions are used to represent experimental enthalpy data. Similar to PVTN EOS, enthalpy constitutive equations are valid over certain ranges of temperature and pressure. For both of these fluid properties, two dimensional tables can be created which give the value of density and enthalpy across the operating pressures and temperatures of the salt separation vessels.

Therefore, by combining the five equations from the fundamental conservation laws (continuity, momentum in three directions, and energy), and known values for density and enthalpy, there are now five equations with five unknowns (T, P, u, v, w). In

the case of the separator vessel, the pressure is actually held constant at all times, so the four variables which must be solved for are T, u, v, and w for each control volume.

3.2 Discretization of Governing Equations

The governing equations presented in Section 3.1 are of the continuous form and can be solved analytically only for the most simple of cases. In order to implement these equations in the finite element model, where each control volume varies in size and shape, it is necessary to first write the governing equations in a discrete form. In order to do this, we first integrate across each control volume. Knowing that the governing equations are written from the Eulerian perspective (i.e., element nodes do not move with the fluid particles, but rather stay stationary as the fluid flows), then the equations can be written:

$$d/dt \int_V \rho \, dV + \int_S \rho \, \mathbf{u} \bullet \mathbf{n} \, dS = 0 \tag{10}$$

$$d/dt \, d/dt \int_V \rho \, \mathbf{u} \, dV + \int_S \rho \, \mathbf{u} \, \mathbf{u} \bullet \mathbf{n} \, dS = \int_S \boldsymbol{\tau} \bullet \mathbf{n} + \int_V (\text{Velocity Source}) \, dV \tag{11}$$

Also, using the Reynolds Transport Theorem for a passive term, an equation is:

$$d/dt \int_V \rho \, \varphi \, dV + \int_S \rho \, \mathbf{u} \varphi \bullet \mathbf{n} \, dS = \int_S \nabla \varphi \square n \, dS + \int_V (\text{Source term}) \tag{12}$$

where φ is passive variable

In order to solve for the unknown values in a discrete equation, consider first the fundamental structure of a finite element control volume that is expressed by the arrangement of the element faces. Each finite element control volume, whether six sided (hexahedral), five sided (wedge), or four sided (tetrahedral), is constructed of a number of

element faces. An example of a three sided, non-symmetric element face is shown in Figure 4.

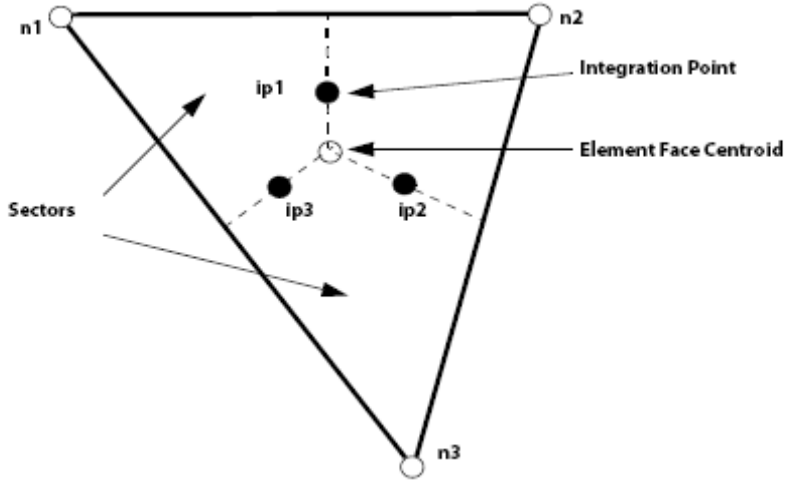

[1]

Figure 4 Three-sided Non-symmetric Element Face

In this figure, the vertices are defined as nodes, the element face center is the intersection of perpendiculars drawn from each side, and the integration points (ip_n) are geometric center points between the element face center and the intersection of the perpendicular and the side. The sectors are the sub-regions of the face element. In order to solve the governing equations across a control volume, source terms are approximated for each sector and then integrated over all control volume element faces. Fluxes are approximated at each integration point and then integrated over all control volume element faces. The equations take the discrete form (assuming a First Order Backward Euler scheme):

$$V(\rho-\rho_o)/\Delta t + \sum_n (\rho \, \mathbf{u} \, \Delta n)_n = 0 \qquad (13)$$

$$V(\rho\mathbf{u}-\rho_o\mathbf{u}_o)/\Delta t + \sum_n (\rho \, \mathbf{u} \, \Delta n)_n \, \mathbf{u}_n = \sum_n (\boldsymbol{\tau} \, \Delta n)_n + (\text{Velocity Source Averaged over Volume})$$

[1] From ANSYS CFX Help Manual, Release 10.0: Theory, p. 241.

(14)

$$V(\rho\varphi-\rho_o\varphi_o)/\Delta t + \sum_n (\rho \mathbf{u} \Delta n)_n \varphi_n = \sum_n (\nabla\varphi \Delta n)_n + (\text{Source Average over Volume})$$

(15)

where ρ_o, $\mathbf{u}_o$, φ_o are the values at the previous time step

The First Order Backward Euler scheme can be replaced with more precise approximations of the equation terms to yield a solution which has a higher order of accuracy. For example, the Second Order Backward Euler scheme applied to the first term of the discrete continuity equation is:

$$V(1.5 \rho - 2\rho_o + 1.5\rho_{oo})/ \Delta t$$

In practice, finite element techniques which are of higher order accuracy will require much greater computational time. Various approximation techniques have been implemented for the terms in the governing equations. The selection of the approximation terms are based on finite element research and computational experience of the finite element method implementer. Though many of the approximation techniques were devised before the advent of computers, considerable research has been dedicated to accuracy, robustness, and computational effort. Finite element models and numerical solutions have been used in industry and academia for decades, and as computer processors and storage capabilities have increased, so to have the accuracy of results.

3.3 Additional Theoretical Considerations

Other important issues that must be vetted to adequately perform the numerical simulation of SALSAN and Konti-2 include issues of near wall mesh geometry, heat transfer deterioration in supercritical flows, and turbulence model accuracy for

supercritical flows, etc. (see refs [5], [13], [17]). In order to adequately perform the numerical simulation of SALSAN and Konti-2, all of these issues must be vetted. The results of previously reported analyses were used to select an appropriate model for the supercritical fluid, flow-reversal scenario.

3.3.1 Turbulence Models and Reynolds Averaging

Turbulent flow is always unsteady in time, and therefore, if one wants to resolve the turbulent flow through numerical modeling, both the grid size and the timescale must be exceedingly small [6]. With the available computational power, this is not normally possible. Therefore, a method of reducing computational time while still finding a solution has been formulated. This method combines the idea of Reynolds Averaging and Statistical Turbulence Models, of which many exist. Turbulence models have been formulated which are meant to supplement the governing equations (Reynolds Averaged Navier-Stokes (RANS) equations and continuity equation).

Reynolds Averaging is a method by which the small time scale of turbulent fluctuations are averaged out in such a way that the mean contribution of the turbulent effects to the flow are not lost, but without actually solving the fluctuations in the flow. The Reynolds Averaged Navier-Stokes (RANS) equation, which is an ensemble averaged equation, due to the averaging, does not contain all the information of the continuous Navier-Stokes equation. Turbulence models provide averaged-out values back into the equation and attempt to capture the chaotic, random, and irregular characteristics of turbulent fluid flow. The RANS equation contains a term named the Reynolds stress tensor, an additional stress term caused by turbulence, the value of which is not known. Turbulence models, regardless of complexity, provide a way to solve for the value of the stress tensor (the shear stresses caused by fluctuating velocities, or turbulence (or Reynolds stresses), in effect providing equations which solve for six of the 10 unknown variables (six shear stresses) and leave the remaining velocity components and pressure, which include only the mean flow properties. Turbulence equations have been derived for different types of simple flows (flow over a flat plate, flow in pipe, low-Reynolds

number flows etc.), and by different groups who used different assumptions or physical reasoning. The accuracy of the equations in differing conditions can be extremely limited. Studies have been performed which addressed the accuracy of various turbulence models. Unfortunately, though many of these address supercritical fluid flow, near wall turbulence, and buoyancy effect, they do not address any steady state solutions for processes with flow reversal or the possibility of re-circulating eddies. The applicability of any one turbulence model must be closely scrutinized before determining it to be an appropriate model. Various turbulence models are tested during the numerical simulations and the results are presented in Chapter 4.

3.3.2 Near Wall Mesh Refinement

Previous experiments and reports indicate that the near wall region in supercritical fluid flow problems is vitally important to the heat transfer solution, and by extension, the entire solution [5]. Roelofs, et al. (2004) [29] performed a numerical study to address the impact of mesh refinement in the near wall region on the accuracy of numerical solutions. The near wall refinement is best evaluated by a non-dimensional parameter, y^+, which shows the relationship between the distance from the wall to the first node and the shear stress. The y^+ is defined as:

$$y^+ = \rho * y * u_\tau / \mu \tag{16}$$

ρ = density (kg/m^3)
u_τ = shear velocity (m/s)
y = normal distance from node to wall (m)
μ = dynamic viscosity (Pa * s)

The definition is clearly dependent on the fluid properties (ρ and μ) for the near wall region and therefore y^+ will not be a constant value at the vessel wall. It is important that the value of y^+ be evaluated at every point along the vessel wall in order to ensure that mesh refinement will adequately capture the strong buoyancy and acceleration effect

which occurs in this region. Establishing an adequate value for y^+ at all locations on the vessel wall is difficult and, with the meshing software that is available, requires that the entire vessel wall have a very fine near wall mesh. Implementation of this fine mesh does impact computation time but is necessary for a good solution.

3.3.3 Heat Transfer Deterioration Effect

The heat transfer deterioration effect, a phenomena observed at specified heat flux rates with supercritical fluids, is a recognized and analyzed, though not necessarily understood, physical event which occurs between solid bodies and supercritical fluids [17]. Experiments have shown that, at a solid/supercritical fluid interface, the heat transfer coefficients increase at low heat flux and decrease at higher heat flux [36]. The phenomena causing this experimental observation is unknown, but studies have been conducted to determine the heat flux ranges over which the phenomena occurs. The range for heat transfer deterioration initiation has been calculated experimentally through mass flux/heat flux comparisons and reported at heat fluxes between 1050 kW/m^2 and 730 kW/m^2, and also estimated using numerical methods as 900 kW/m^2. [29,36]. If the heat flux at a supercritical fluid/solid interface is in this range, it is expected that the heat transfer coefficient will decrease and therefore heat transfer from the solid to the fluid will be less than heat transfer calculations predict. The result is that heat transfer calculations incorrectly predict temperatures when the heat transfer deterioration effect is occurring. Although the heat transfer flux was not measured during the experimental runs with SALSAN, numerical simulations indicate that the maximum heat transfer flux at any point on the vessel wall is near 500 kW/m^2, which is less than the reported values for commencement of heat transfer deterioration. Therefore, the heat transfer deterioration effect can be excluded as a source of error for the numerical simulations.

4. Materials and procedures

4.1 Physical Experiment

The reverse flow, brine pool salt separation vessel is only one portion of the entire catalytic conversion process. Figure 3 shows a schematic for the experimental separation process as set up at the Paul Scherrer Institut in Switzerland.

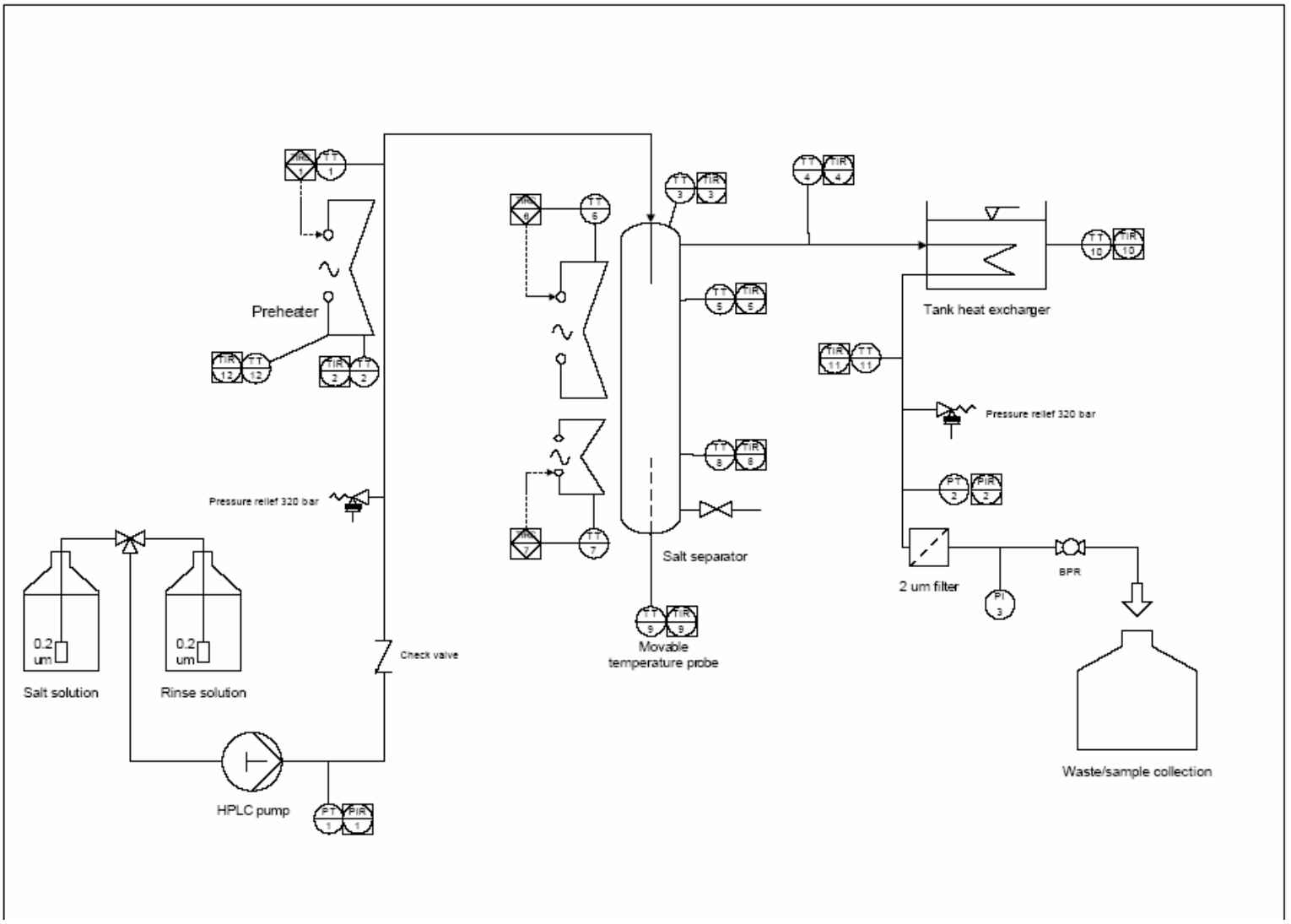

Figure 5 Experimental Salt Separation Set-up

The experimental set-up used to test the salt separation process separately from the gasification process is shown in Figure 5. Instead of a biomass solution, a simplified salt solution is injected so that the focus is on the salt separation process in a well controlled environment. The location of the actual solid-salt solution separation is the center vessel. The attached peripherals (heat exchanger, filters, pumps, etc.) support the process in that they provide the feed to the reactor vessel at the correct temperature and pressure. Two heaters on the reaction vessel maintain temperature's at the desired level. The computer model will exclude all peripherals and set vessel boundary conditions as would occur in the laboratory experiment.

The salt separator vessel is a narrow, metallic, cylindrical tube which can operate at temperatures and pressures at and above the critical point of water. In the experimental system, salt solution is injected via a needle-like dip tube into the separation vessel through a small opening at the top of the vessel. As currently designed, the inlet flow is at sub-critical temperature, but the inlet temperature can be easily varied through the use of a pre-heater. The vessel itself is heated to supercritical temperatures (near 450 °C) in the upper two-thirds (approximately 0.27 meters) and at sub-critical temperatures (approximately 310 °C) in the lower third of the vessel (remaining 0.13 meters).

Figure 6 SALSAN Reaction Vessel, approximate length .4 meters

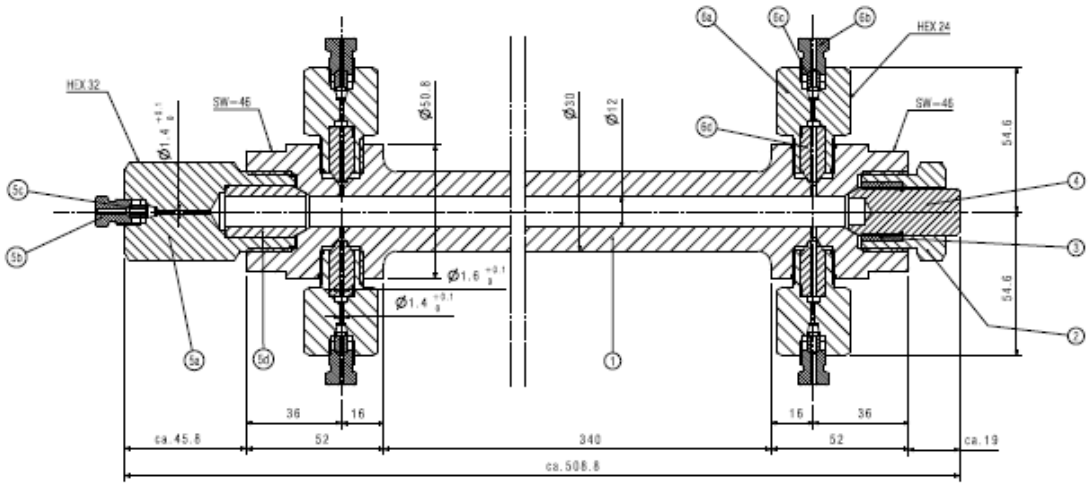

Figure 7 SALSAN Schematic (inlet to left, measurements in centimeters)

The salt solution, which is at supercritical pressures (P = 300 bar) but introduced at sub-critical temperatures, will experience extremely rapid changes in thermo-physical properties as it is heated to a super-critical temperature. Interestingly, the density of the pure water supercritical fluid will vary significantly from as high as 1010 kg/m^3 ,at 25 °C and 300 bar, to as low as 150 kg/m^3 , at temperature = 450 °C and 300 bar. This rapid change in density will affect the fluid velocities, and experience shows that buoyancy forces will eventually overcome gravitational forces and the downward flow of the supercritical fluid will reverse and flow upward. Figure 8 shows a possible velocity flow field in the vicinity of the injection needle exit (where fluid initially enters the reaction vessel). The figure shows fluid flow in both the upward and downward direction and also a flow reversal region.

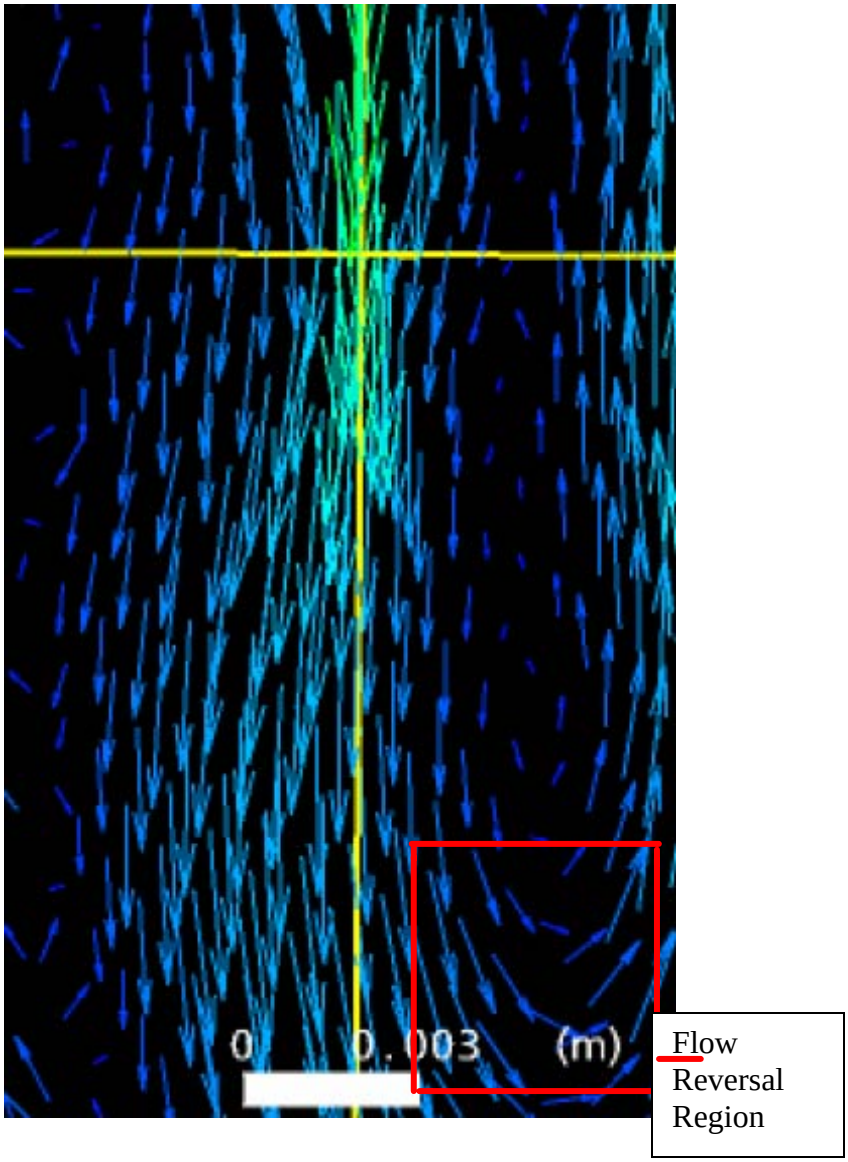

Figure 8 Possible Fluid Flow vector plot, showing flow reversal (intersection of yellow lines shows inlet location)

Therefore, the process for the salt separator is to introduce the water and biomass solution at sub-critical temperatures, ranging from 25 to 250 °C at 30 MPa, and then allow heat transfer from the inner vessel wall maintained at supercritical temperatures, to heat the salt solution to temperatures exceeding the critical temperature. As the solution is heated, salt solubility will decrease dramatically as the water enters the supercritical region where salts will precipitate out of the solution. Additionally, the density of the fluid, will decrease rapidly, causing an increase in buoyancy, and flow reversal will occur.

4.2 Numerical Modeling

Similar to physical experiments, the tools used for numerical modeling are vital to the success of the study. The spectrum of simulation tools can be divided into two major parts, a) the software system, and b) the hardware system. The software must be understood at both a general level, with issues which apply to any type of numerical modeling problem, and at a specific level, with issues which apply specifically to Computational Fluid Dynamics problems and even more specifically to supercritical fluid conditions. The hardware system contains issues which must be understood on a general level, or how the hardware is utilized to perform the calculations ordered by the software. The coupled interaction of the general software and hardware issues must also be considered.

Although the intent of this research is not to re-invent numerical modeling, it is worth mentioning the different hardware and software systems that were used and a brief comparison of the different experiences with each set up. Research labs do exist which perform only computer based experiments. These labs often work in conjunction with a physical experimenting lab, but have separate budgets and different personnel with different backgrounds, educations, and areas of expertise. The result is two different labs which compare the results of their research - one set of results which comes form physical experiments and one set of results which from numerical simulations. The researchers performing the numerical experiments are known for their experience and expertise with finite elements models, computer systems, and modeling of certain physical systems, i.e. structural analysis, hydrodynamic analysis, etc. Expertise in the area of structural analysis does not always translate to expertise in the area of hydrodynamic analysis.

All these things considered, numerical simulations that are conducted as complimentary research in a primarily physical experiments' lab may be at some inherent disadvantage. These disadvantages will not prevent one from arriving at the correct solution. There is, however, a substantial learning curve which must be considered when

numerical simulations are undertaken. Unlike a purely computational lab, there may not be in place computers, software, and operating systems which are already optimized for numerical simulations. A significant portion of the work in finding a numerical solution to compare to empirically arrived data is the selecting, purchasing, configuring, and testing of the optimum computer system within the time and budgetary constraints of the study.

Finite Element Analysis Software must be robust and able to process a variety of different physical problems. For a chemical engineering application, the potential phenomena that needs to be represented are oxidation, combustion, hydrolysis and other chemical reaction processes, pipe flow, fluid phase change, simple structural loading (for example a high pressure system in a cylindrical vessel), fluid flow, and heat convection, radiation, and conduction. There are some types of commercially available software packages, which, due to their complexity can treat these issues but they are all relatively expensive. Choosing a software package which optimizes capabilities while staying within reasonable fiscal constraints is important.

4.2.1 Available Computer Modeling Software - Specific Software

A wide variety of computational fluid dynamics software is available for performing the numerical modeling of a supercritical water process. Of those available, there are three which have gained relatively high use by researchers and private industry. These three software packages are COMSOL (formerly FEMLAB)[8], FLUENT [20], and ANSYS CFX. Each one of these software packages has been used to perform model simulations for different groups (labs, researchers, private industry, government, etc), with results accurate enough for publishing.

Since all three software packages have been used in the past for modeling super-critical water processes, the selection of a software package becomes a subjective process versus evaluation of capabilities. A cursory review of the three different types of software was conducted, resulting in an opinion that ANSYS CFX is the most user

friendly and intuitive software. Defining boundaries and specifying boundary conditions are simple to implement, different material models are built into the software, as are multiple options with regards to turbulence models (12 different types of turbulence models are available), fluid properties, etc. "Help" menus and tutorials are thorough, however perhaps not to the depth of detail that will be required for the salt separation modeling. (This exact issue is mentioned in multiple articles, where statements are made about "modifications" to software code in order to properly model supercritical fluids.)

Once a software package is chosen, an in-depth study of the inner workings of the software is necessary to determine how the software reaches a solution. The drive to perform this analysis is to ensure that the software does not become a "black box", where initial conditions are input and results appear as output. Rather, it is important to understand what methodology the software uses in reaching a solution. This will ultimately lead to a better ability to analyze results and quantify uncertainties and thus place more confidence in the accuracy of the simulations.

In general, all CFD software functions with a similar approach or methodology. The modeling problem is "meshed", or broken into finite control volumes, and then the governing equations are solved for each control volume. These equations include the continuity equation, momentum equation, and energy equation as presented in Chapter 3. Additionally, an equation of state for the density values and constitutive relationship for enthalpy values are utilized. For CFD, it is extremely important that the Equation of State and constitutive relationship are accurate over the range of modeled temperatures and pressures. CFD solutions found using the three governing equations can be no more accurate than the values for density and enthalpy provided by the EOS and constitutive relationship. Previous versions of CFX software provide EOS which are not accurate in the supercritical region for water. The newest version of CFX, 11.0 does include density and enthalpy values for water that are calculated using the International Association for the Properties of Water and Steam Industrial Formulation 1997 (IAPWS IF-97). These standard water property values are accurate (within 3%) for the operating ranges of the SCWO process (up to 30 MPa and 1000 °C) and are therefore extremely beneficial for

use in the model. Since the impact of salt and carbon compounds on the thermo-physical properties of the fluid are hard to predict, initial modeling will be performed with pure water. Therefore, the accuracy of these water property values are important as they impact the accuracy of results.

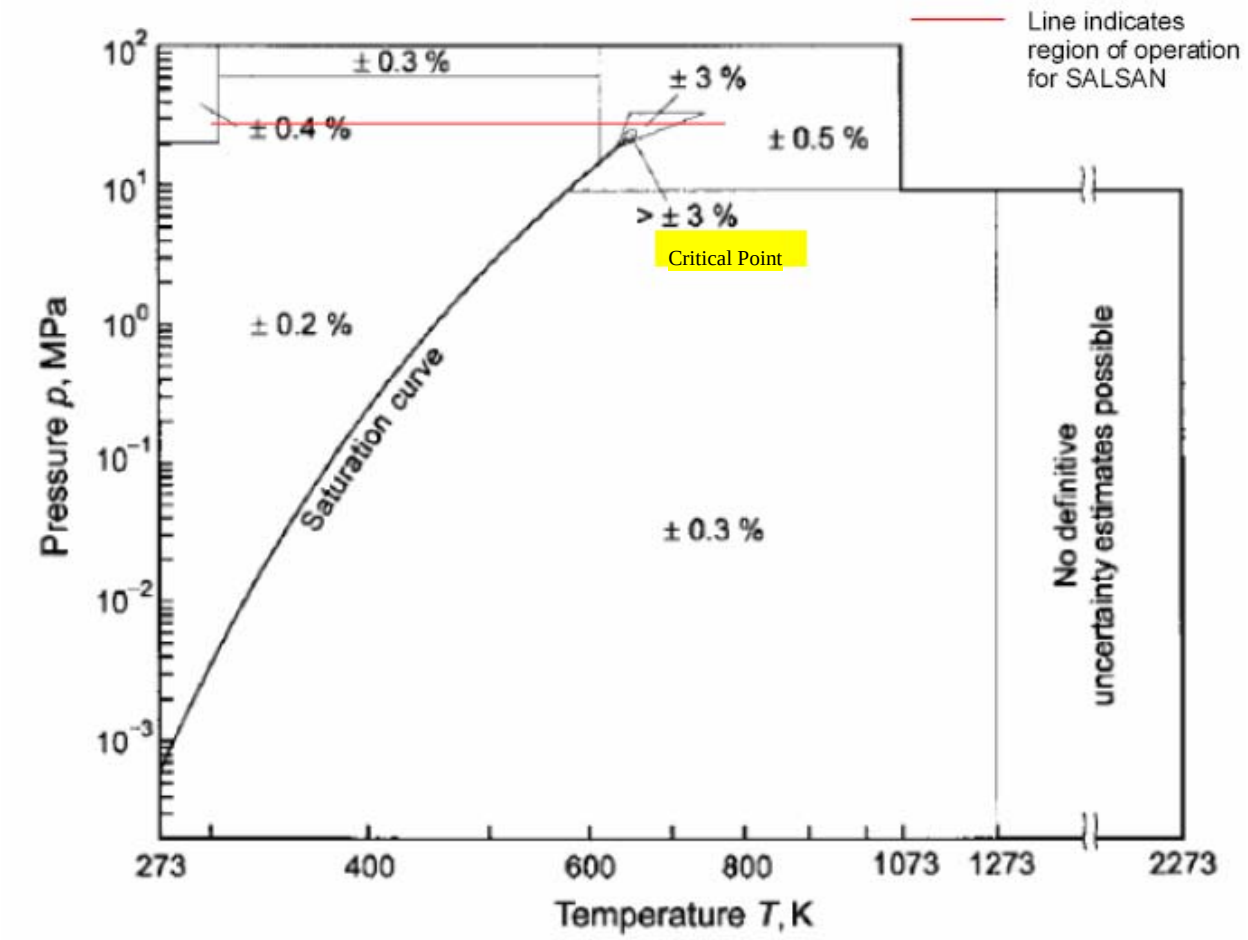

Figure 9

Figure 9 shows the uncertainty for the IAPWS-IF97 calculated isobaric heat capacity on a Pressure and Temperature grid. For reference, the saturation curve and critical point are labeled. Although the regions of greatest uncertainty exist in the sub-critical to supercritical transition zone, the IAPWS-IF97 is considered the most accurate Equations of State for pure water. [35]

The computer modeling software, though multi-functional and extremely powerful, does not yield acceptable results without understanding the solving process and introduction of correct boundary conditions. The inputs into the computer model must accurately present the real-world experimental process in order to yield a credible solution. This is a challenge, since part of ANSYS CFX's attractiveness, the multi-

variability with a variety of modeling possibilities, can become a hindrance if not properly managed. Considerable resource and time must be allotted to understanding all functionalities.

4.2.2 General Software - Operating Systems

For many computer applications performed by the everyday computer user, rarely is a software error simply the result of using one operating system over another. For instance, rarely does a user find that they can perform a word processing function using only Microsoft Windows XP or only a version of Linux/Unix. These programs, which do not demand a large amount of computer resources, are not affected by the Operating System. For more computationally intensive software, or more specifically software which requires access to a large amount of Random Access Memory to perform many calculations, there are important differences in how Operating Systems affect operation of a software package. Although the limitations and reasons behind them are numerous, and also much better understood by computer experts, there are simple lessons that can be applied when selecting a single processor system to be used for numerical simulations.

The software review conducted in this investigation should not be considered an exhaustive scientific study to find the absolute best computer system for numerical simulations. That question can be better answered by Finite Element Analysis researchers who dedicate the majority of their research time and money on improving their computational ability (improving in terms of speed, size, etc.) This review, rather, is based on first-time user experience in the context of setting up numerical simulation software at a reasonable cost (in terms of both computer hardware, software, and software licenses) for a relatively complex and computationally intensive problem. The assumption is that users may want to set up numerical simulations which complement their physical experiments, but have a limited budget and limited time to configure the computer system.

For a user with limited knowledge or experience performing numerical simulations, there exist a multitude of sources of information. Of those multitude, the sources with the combination of best information and lowest risk are the software provided help files and the software supported user forum. The user forum is a webpage resource operated and maintained by the software production company. It allows end users, mainly engineers and researchers who use the software on a regular basis, to share experiences, knowledge, successes, and failures. This expansive resource is highly beneficial, as long as user's opinions and experiences are considered in the correct context and no single posting is considered absolute fact until verified.

Upon commencing the salt separation numerical study, initial information regarding both software and hardware segments of the computer set up were gathered from the software help files and the user forum webpage. The two different sources give very different information regarding a "proper" machine set up. The software help files, written by the software production company, are written for a very broad audience. The standard format for software producers (possibly an attempt to reduce customer alienation) is to provide a listing of the minimum hardware necessary to operate a software package. This minimum requirement rarely correlates to a system which will perform well over a broad spectrum of software abilities. Furthermore, the user files do not provide any information about the positive (or negative) impact of hardware upgrades. The user forum, fortunately, does contain some guidance regarding hardware and software interaction. Through thorough data gathering, hardware and software interaction can be understood and, given a set of economic constraints, an optimum system can be configured. The important element is software performance improvement as a function of cost. Understanding where money is spent, on what specific hardware upgrades, is most beneficial and will result in a computational machine which will perform to expectations.

Three different operating systems were utilized in the completion of the numerical study. The Windows Operating System was initially used as it was readily available and familiar to the user. Red Hat LINUX Operating System was chosen for installation in a

newly purchases computer following initial testing on the Windows system. Negative experiences with Windows, combined with anecdotal evidence available from numerous sources of experienced computer users, drove the decision to install Red Hat LINUX over the more familiar, and more ubiquitous, Windows. The user help files also chronicle some memory limitations with 32 bit Windows OS which are difficult to overcome. The Red Hat version of LINUX (of which there are many different variants available) was chosen because of the local support available. It was not chosen due to known superiority when compared to other LINUX Operating Systems.

Operating system, RAM, processor, Pros, Cons, results

Operating System/Processer/ RAM	Largest nodes processed	Benchmark time	Pros	Cons
Windows XP/Pentium 4 2.4 GHz / 512 MB	Not tested.	315 secs	Installation and license management simple	Very poor speed performance. Substantial limits on size of mesh file.
LINUX Red Hat 32 bit/ Dual Core XEON Processor, 3.2 GHz/4 GB	1.2 Million	167 secs	Improved speed performance, all RAM accessible	Installation a little more difficult; license management is initially more challenging and requires time and increased depth of knowledge
LINUX Red Hat 64 bit/ Dual Core XEON Processor, 3.2 GHz/4 GB	2.3 Million	155 secs	Improved speed performance over 32 bit installation, handles larger meshing files, executes with finer discretization in boundary layer zone	

Table 1 Simplified Computer Configuration Comparison

The experience gained in this part of the study indicated that the better Operating System (OS) for numerical simulations is the Linux Operating System. The Linux OS allows the computer to access all available RAM in order to perform computations. This translates to a more finely meshed geometry. Although extensive testing of Windows XP was not performed, it is known that Windows XP OS does limit the accessible RAM for an application. Previous operation with computationally intensive software has yielded

the manifestation of this problem. This limitation can be over-ridden, but it is not a trivial process and can be intimidating to a novice user. The 64-bit version of Windows XP does allow all RAM to be accessible, but in a cost comparison of freeware Linux OS ($0) versus Windows XP 64-bit (greater than $0), the Linux OS is superior. Additionally, the Linux Operating Systems allow for much greater control of many aspects of the computer. While this may seem to be burdensome when first starting with Linux, experiences during the completion of this numerical study showed the additional control to be invaluable.

If available, a 64-bit Linux OS is preferable to a 32-bit Linux OS. The 64-bit architecture enables the software to access a larger amount of memory simultaneously than the 32-bit architecture. The 64-bit OS allowed the use of larger meshing files with finer discretization in the boundary layer region. This improvement in boundary layer region refinement yields an order of magnitude improvement in the solution.

4.2.3 Benchmarking of single processor system

A benchmark file is included in the software installation and can be utilized to judge the speed/efficiency of a user's system. These types of comparisons are important to determine if the money and time dedicated to building a good numerical simulation machine were well spent. In other words, how does the instrumentation built for these simulations compare to machines in other similar simulations. The benchmark computational times reported by other users on the ANSYS CFX website, for single processor machines, are (dates are important as computer processor speed and cost change rapidly over a period of six to twelve months):

DATE	OS/Processer/RAM	Total Time
3 Aug 2006	LINUX SuSE Pro 9.1 64 bit/ AMD Operton 246 2.0 GHz, 1 GB	202 sec
26 September 2006	Windows 64 bit OS / Woodcrest 5160 CPU 3. GHz / 8 GB	115 sec
2 Oct 2006	64 bit (OS not provided) /Opteron Dual Core 2.0 Ghz / 8 GB	176 sec

Table 2 Computational Speed Comparison

Comparing these data points to the above listed processor time of 155 seconds on the 64 bit Linux Operating System indicates that the hardware and software configuration chosen for this study is adequate. Although the 64 bit Linux OS configuration did not outperform the 64 bit Windows OS (with Woodcrest processor), the Windows OS had a 2:1 RAM advantage, which will significantly impact computational speed. The two OS's are not evenly compared since they are using two different hardware systems. Regardless, the benchmark tests do show that the computer configuration used for the numerical simulations does perform well.

The time recorded for the 64 bit, Red Hat Linux on the Xeon processor with 4 Gigabytes of RAM is 155 seconds. The time recorded for the 32 bit, Red Hat Linux on the Xeon processor with 4 Gigabytes of RAM is 167 seconds. This indicates that the upgrade from a 32 bit OS to a 64 bit OS, in addition to the improved mesh refinement capability, will also yield a speed improvement near 8%. This may not seem like a large improvement, but considering that simulations were run on the machine for at least 145 days, an estimated 12 days of simulation time was saved.

5. Results and Discussion

Orientations, definition of axes: In order that the results discussion can be easily understood, the coordinate axes is defined visually in Figure 10.

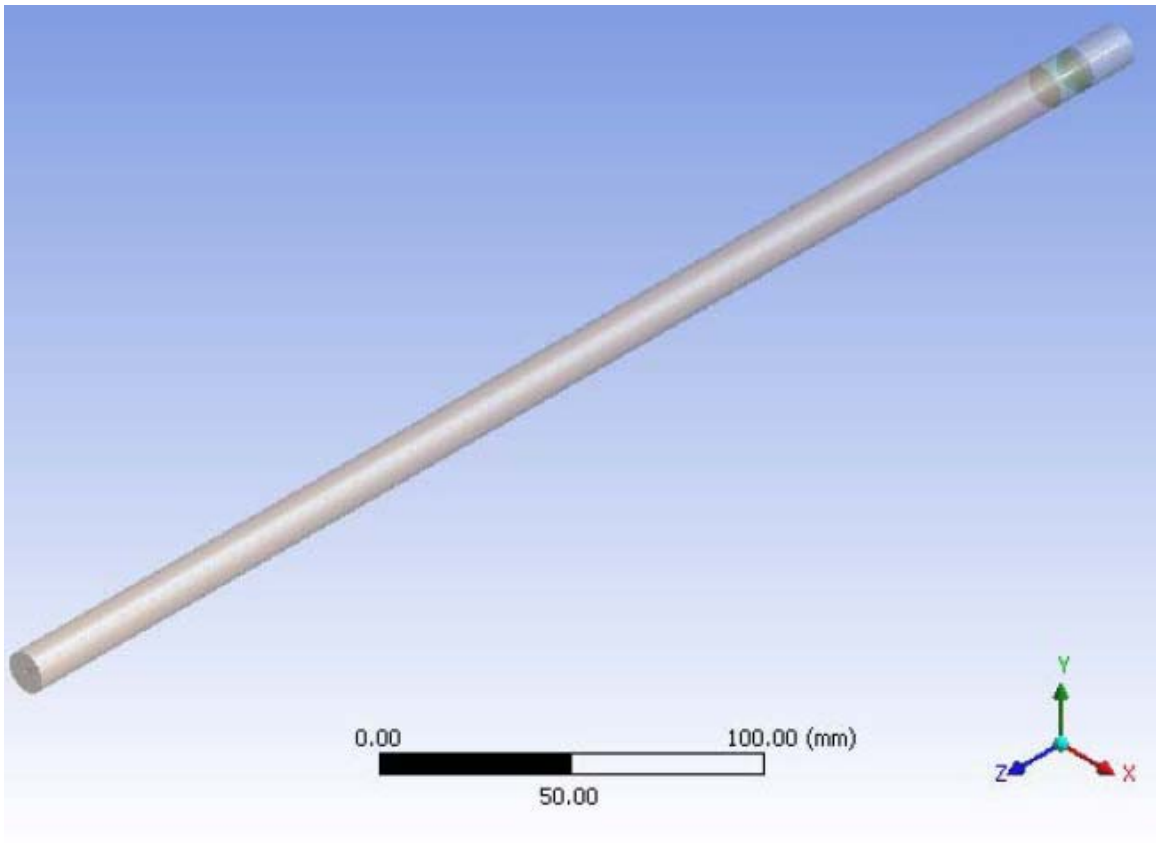

Figure 10 CAD Showing SALSAN Geometry

In the orientation used for the numerical simulations, the inlet of the injection tube is at the top of the geometry at z = 0. The center of the circle which defines the cylinder is at (x=0,y=0). The outlet of the separation vessel is at (.006,0,.016) meters, but is not visible in the above representation of the geometry. The z orientation was selected such that distance from the inlet increases as z increases. The gravitational constant in this case is positive, and positive "w" velocities correlate to downward fluid flow and negative "w" velocities correlate to upward fluid flow.

5.1 Solution Validity Determinations

In the process of performing these numerical simulations, there are two methods to determine if a result is a "good" solution. The first method is to analyze the output of the numerical calculations. Comparing the output of the numerical calculations will help determine the precision of the mathematical model. The second method is to compare the numerical results to empirical data. The results of this comparison will indicate if the mathematical model properly represents the physical process.

5.1.1 Output of numerical calculations.

"The residual is a measure of the local imbalance of each conservative control volume equation. It is the most important measure of convergence as it relates directly to whether the equations have been solved"[2]

The residual value is a representation of the precision of the solutions found for each control volume. (In the finite element methods, one value of temperature, pressure, velocity, etc is assigned to each control volume, or mesh element.) The solutions are to the three governing equations, in their discrete form, as shown in Chapter 3. In order to determine the model residual values, the solutions of temperature, pressure, and fluid velocity are calculated for each control volume. The difference between the left hand side and the right hand side of each discretized governing equation for each control volume is defined as the residual value for that control volume. In the case of the normalized residual[3] values calculated in CFX, the convergence criteria are defined as:

---

[2] ANSYS CFX, Release 11.0: ANSYS CFX-Solver Modeling Guide, Advice on Flow Modeling, Monitoring and Obtaining Convergence

[3] Normalized residual values are unitless. For each solution variable, ϕ, the normalized residual is given in general by:

$$[\tilde{r}_\phi] = \frac{[r_\phi]}{a_p \Delta\phi}$$

where r_ϕ is the raw residual control volume imbalance, a_p is representative of the control volume coefficient and $\Delta\phi$ is a representative range of the variable in the domain. The normalization ensures that a small raw residual which is the result of a small variable value (for example .001 or less) does not yield a false sense of convergence.

- Greater than 5e^-5: very poor, global balances will be poor and quantitative data is largely unreliable.
- 5 e^-5 is loose convergence
- 1 e^-5 is good convergence, often good enough for most engineering applications
- 5 e^-6 is tight convergence

The aggregate residual value for any one variable is the integration of the variable's individual control volume residuals divided by the total volume. This aggregate residual is simply a volumetric average of the error over the entire volume, which means that some elements will have higher residual values and some elements will have lower residual values. Determining the regions of high and low residual values can sometimes be helpful in evaluating the numerical solution. Table 3 shows example residual value output from CFX for one iteration.

OUTER LOOP ITERATION = 59 CPU SECONDS = 3.370E+04

Equation	Rate	RMS Res	Max Res		Linear Solution	
U-Mom	1.01	2.6E-04	4.9E-03		1.0E-02	OK
V-Mom	1.01	2.6E-04	5.4E-03		1.0E-02	OK
W-Mom	1.00	7.8E-05	1.2E-03		1.4E-02	OK
P-Mass	1.00	4.7E-08	4.7E-07	5.1	2.9E-03	OK
H-Energy	0.96	1.8E-04	1.9E-01		1.4E-02	OK
T-Energy-Needle	0.84	1.5E-04	8.8E-04		1.4E-02	OK
T-Energy-Titanium	1.03	2.0E-05	6.6E-04	5.8	1.4E-02	OK
K-TurbKE	1.03	4.6E-06	8.6E-04	5.9	3.8E-02	OK
E-Diss.K	1.08	6.6E-06	1.2E-03	7.2	8.0E-03	OK
P-Mass	0.06	2.7E-09	3.8E-07	5.1	3.1E-03	OK

Table 3 Example Residual Value Output

The "RMS Res" value is the root mean square normalized aggregate residual value. The "Max Res" value is the maximum residual value amongst all the elements in the volume. There are additional analysis techniques which can be utilized to compare multiple numerical simulations and try to estimate an overall error estimate for the simulation. These techniques require substantial computer memory and will be discussed further below.

5.1.2 Comparison to empirical data. In the case of SALSAN, there are three sets of empirical data which can be used for validation purposes. Temperature readings as a function of longitudinal length (assumed to be taken at the radial center of the cylinder) were taken for three different fluid flow rates: 1 mL per min, 5 mL per min, and 10 mL per min. There is a large dependency on Reynolds number and the region of operation for the process. Ironically, initial experimental runs of SALSAN were performed at 10 ml/min, 5 ml/min, and 1 ml/min. For the dimensions of the SALSAN separator vessel, dimensions of the inlet needle, dimensions of the separator vessel, and the operating fluid properties, it is assumed that the Reynolds number will vary greatly throughout the solution field. Estimated Reynolds number (assuming incompressible flow in the needle dip tube) for these flow rates are given in Table 4. Initial simulations show that solutions can be strongly dependent on Reynolds Number.

SALSAN P (bar) 300

	Inlet flow rate	Inlet Temp	Density	Mass Flow rate	Diameter	viscosity	Max Speed In possible	Max Re number
10 mL/min	mL/min	[K]	[kg/m^3]	[kg/s]	[m]	[Pa*s]	[m/s]	
Inlet	10	298	1010	0.00016836	0.0008	0.00088823	0.331	302
Vessel	10	642	583	9.7246E-05	0.012	6.7593E-05	0.331	34364
1 mL/min								
Inlet	1	298	1010	1.6836E-05	0.0008	0.00088823	0.0331	30
Vessel	1	688	223	3.724E-06	0.012	3.3637E-05	0.0331	2644
5 mL/min								
Inlet	5	298	1010	8.418E-05	0.0008	0.00088823	0.1658	151
Vessel	5	670	399	3.3242E-05	0.012	4.777E-05	0.1658	16621
1000 mL/min								
Inlet	1000	453	905	0.01508708	0.0008	0.00015724	33.174	152790
Vessel	1000	576	745	0.01242804	0.012	9.2144E-05	33.174	3221550

Table 4 Flow conditions and properties and calculated Reynolds numbers

For fluid flow in the separation vessel, based on Reynolds number for flow in a tube, is:

$Re < 2000$ Laminar flow
$2000 < Re < 4000$ Transition Regime

Re > 4000 Turbulent flow

where $Re = \rho D u / \mu$

ρ = Density[kg/m^3]
D = Inner Diameter[m]
u = Velocity [m/s]
μ = Dynamic Viscosity [Pa *s]

5.2 Results at Various Mesh Discretizations

Initially, simulations using the properties of both SALSAN and Konti-2 vessels were performed. Specific characteristics of those simulations are shown in Table 5.

	SALSAN	Konti-2
Inlet flow rate (g/s)	.16667	.34447
Inlet Temp (°C)	25	250
Vessel Length (mm)	402	694
Vessel Diameter(mm)	6	6
Inlet Depth (mm)	27	248
Outlet z location (mm)	16.5	35
Wall temp (°C)	0<z<250 mm, 450 205<z<402 mm, 300	0<z<514 mm, 480 514<z<694, 300
Pressure (bar)	300	250
Notes		Cooling water inlet at z = 654 mm, flow rate .0000333 kg/s, additional outlet at z = 694

Table 5 Initial Numerical Simulation Values

Converged solutions, with acceptable residual values, were difficult to obtain for these simulation conditions. Attempts to improve results through various methods showed some success, but did not yield an overall reduction in residual error to acceptable levels. The reasons for this, though difficult to prove beyond uncertainty, can be postulated based on the experiences while conducting the simulations, known issues with finite element models, and results presented by other researchers for similar flow situations. It is suspected that the two largest sources of error in the initial simulations were due to the element meshes (size and shape) and the flow velocity. The errors due to meshing are introduced due to discretization errors (in the case of the mesh size) and possibly dispersion errors (in the case of shape). The flow velocities, combined with the fluid and vessel properties, result in Reynolds numbers which indicate that different flow

regimes exist within the separation vessel. There are regions within the vessel where the Reynolds number is high, inertial forces dominate, and flow is in the turbulent regime. There are also regions where the Reynolds number is low, the viscous forces dominate, and the flow is in the laminar regime. These different flow regimes, and the transitional region that exists between the two, cannot be decoupled in the CFD software. Figure 10 shows the calculated Reynolds number for the four different mesh spacings.

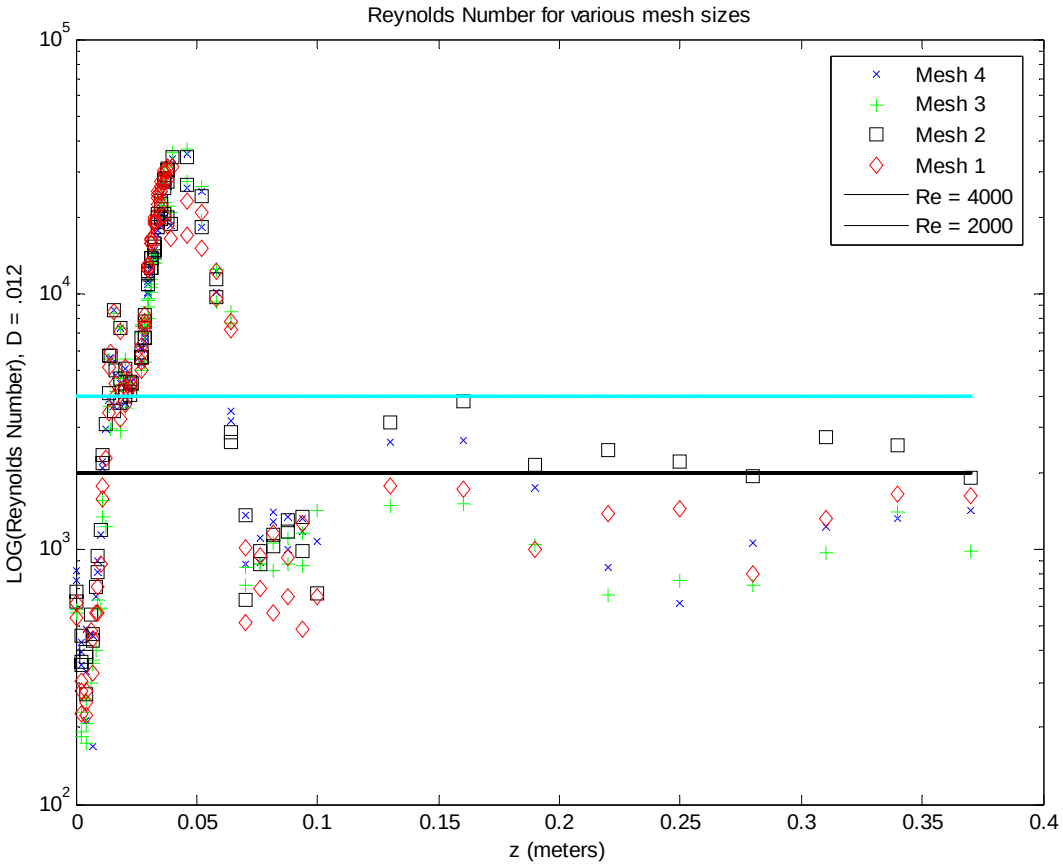

Figure 11 Calculated Reynolds Number Along Length of Separation Vessel (SALSAN)

The Reynolds Numbers shown in Figure 11 indicate that the fluid velocities inside SALSAN will range from turbulent to laminar, and also include velocities in the transitional regime. The impact of using a turbulence model in a laminar regime is unknown but sure to impact the results, as the mathematical model does not match the physical problem. Figure 12 shows an example of the different results obtained for the SALSAN simulations.

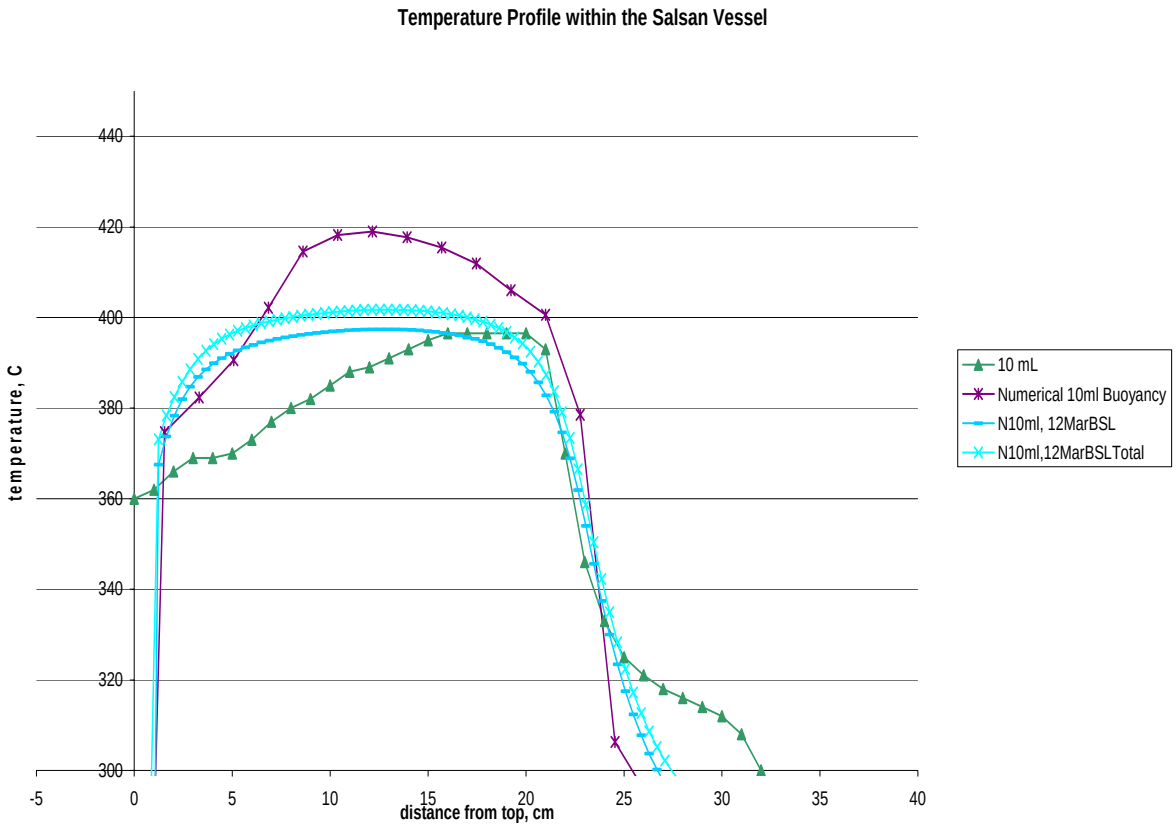

Figure 12 Empirical Data Compared to Numerical Simulations, SALSAN

The "10 mL" curve corresponds to the empirical data, the "Numerical 10 mL Buoyancy" curve is a simulation using a Zero equation turbulence model, and the other two results are simulations using the more complex baseline k-omega turbulence models with one accounting for the regions of high velocity, "N10mL, 12MarBSLTotal", and one which favors the regions of low velocity, "N10mL, 12MarBSL." This plot shows the rather large variation in simulation results when making different physical assumptions.

Following considerable work on reducing the solution error for both SALSAN and Konti-2 at the simulation properties indicated in Table 5, efforts were commenced on achieving a converged solution at a higher mass flow rate. The desired result was a converged solution with which to compare the impact of turbulence models and mesh spacing on results. To that end, four different meshes, each with a successively greater number of elements were constructed and simulations using the standard k-epsilon

turbulence model were completed. Table 6 shows mesh characteristics for the four meshed volumes.

Mesh	Increments in z direction	Number Elements	Number Nodes	Elements per z increment	x and y average length
4	500	420000	420000	840	0.36583889
3	500	780000	770000	1560	0.26845235
2	500	888000	865000	1776	0.25159849
1	375	1736000	1716000	4629.33333	0.1558369

Table 6 Mesh Characteristics (Higher Mesh Number Indicates Larger Mesh Spacing)

The characteristics of the four different meshes are driven primarily by software and hardware limitations. First, there is a limitation in the number of increments that is possible in the z direction where the maximum number is 500. The value of the z increment for mesh 1 was decreased due to the second limitation, the solver computational capability. For the hexahedral meshing scheme implemented in SALSAN, the maximum number of elements that the solver could compute in a reasonable amount of time was near 1.9 million elements. A simulation was conducted with a mesh that contained 2.3 million elements, over a period of 4 days, but results did not dramatically improve.

Unfortunately, due to the attempt to model in three dimensions, the four meshed volumes do not lend themselves very well to any type of standard grid convergence study. In order to perform a true grid convergence study, with a minimum of three meshes (coarse, medium, fine) and equal refinement in all three directions, the medium mesh would require 8 times as many elements as the coarse mesh, and the fine mesh would require 64 times more elements than the coarse mesh. Assuming an upper mesh limitation of 2.5 million elements, the medium mesh would have 312,500 elements and the coarse mesh only 39,000 elements. The coarse mesh would not yield results which could be utilized in a standard grid convergence study. Regardless, comparisons can still be made between the different meshes which yield some insight into the numerical results.

First, consider the residual errors from the four different meshes. Appendix 1 shows maximum residual location, peak residual value, and final residual value for each variable of interest in their specific sections of the reactor vessel (recall the three portions of the model from Chapter 2: injection needle, separation reaction zone, and separation vessel walls). From these simulation results, the variables with the largest residuals are selected for initial analysis.

Mesh 4	Distance	PeakRes[4]	FinalResid[5]	Mesh 3	Distance	PeakRes	FinalResid
U-Mom-Separator	3.49E-01	9.80E-04	2.05E-04	U-Mom-Separator	2.08E-01	4.97E-03	2.34E-04
V-Mom-Separator	3.67E-01	9.92E-04	2.08E-04	V-Mom-Separator	3.22E-01	2.92E-03	2.38E-04
W-Mom-Separator	1.19E-02	9.13E-04	7.62E-05	W-Mom-Separator	1.20E-02	1.20E-02	8.38E-05
H-Energy-Separator	3.75E-01	1.28E-03	1.85E-04	H-Energy-Separator	3.75E-01	4.17E-03	2.37E-04
Mesh 2	Distance	PeakRes	FinalResid	Mesh 1	Distance	PeakRes	FinalResid
U-Mom-Separator	3.05E-01	9.67E-04	2.38E-04	U-Mom-Separator	1.21E-02	2.84E-04	1.37E-04
V-Mom-Separator	2.03E-01	9.35E-04	2.41E-04	V-Mom-Separator	3.75E-01	2.87E-04	1.39E-04
W-Mom-Separator	1.11E-02	6.39E-04	7.96E-05	W-Mom-Separator	3.90E-04	6.03E-04	8.57E-05
H-Energy-Separator	3.75E-01	1.31E-03	2.09E-04	H-Energy-Separator	3.75E-01	8.37E-04	1.05E-04
				E-Diss. K-Separator	4.00E-04	1.21E-02	1.30E-03
				E-Diss. K-TubeIn	4.00E-04	1.69E-03	1.04E-04

Table 7 Mesh Residuals Greater than Desired Convergence Values

All four meshes resulted in velocity residual values which are about one order of magnitude greater than required for an acceptable solution. Also, interestingly, the solution residuals did not improve when upgrading the mesh spacing from mesh 4 to 3, 3 to 2, or 2 to 1. Again, considering that the discretized equations are second order accurate, there is an expectation that the error improves by 50% with each halving of grid

[4] "PeakRes" corresponds to the peak residual value for any one element in the separation vessel.
[5] "FinalRes" corresponds to the final aggregate residual value for all elements in the separation vessel.

spacing. Unfortunately, even from the most coarse to finest grid (4 to 1), the grid spacing refinement only occurs in the x and y direction. The grid refinement in the x and y direction averages out to a little better than halving the x and y grid spacing, but it is not expected that the error is reduced by 50% from mesh 4 to mesh 1.

Of particular note in this study of the highly complex three dimensional flow is the location of the highest residual value. In Table 7, the "Distance" value is defined as the distance from the (x,y,z) coordinate of the element with the highest residual to the exit point of the needle injection tube, (0,0, .027 m). The value is defined in this manner because the area of interest is near the fluid inlet to the vessel, at the needle injection tube exit (z = .027 m). For example, the location of the element with the largest residual for the separator energy term is .375 meters from the region of particular interest. For all four meshes, the distance value for all variables of interest are greater than 100 mm, with the exception of the 'w' velocity, or velocity in the w direction. This fact should be remembered in evaluating the validity of results as additional simulation studies are performed for optimization.

A look at the specific residual values at various locations along the length of the separation vessel aids in locating the regions where the solver is not calculating a converged solution. First, the residual values along the centerline of the vessel, from (0,0,0) to (0,0,.402 meters), for the variables of interest are shown in Figure 13.

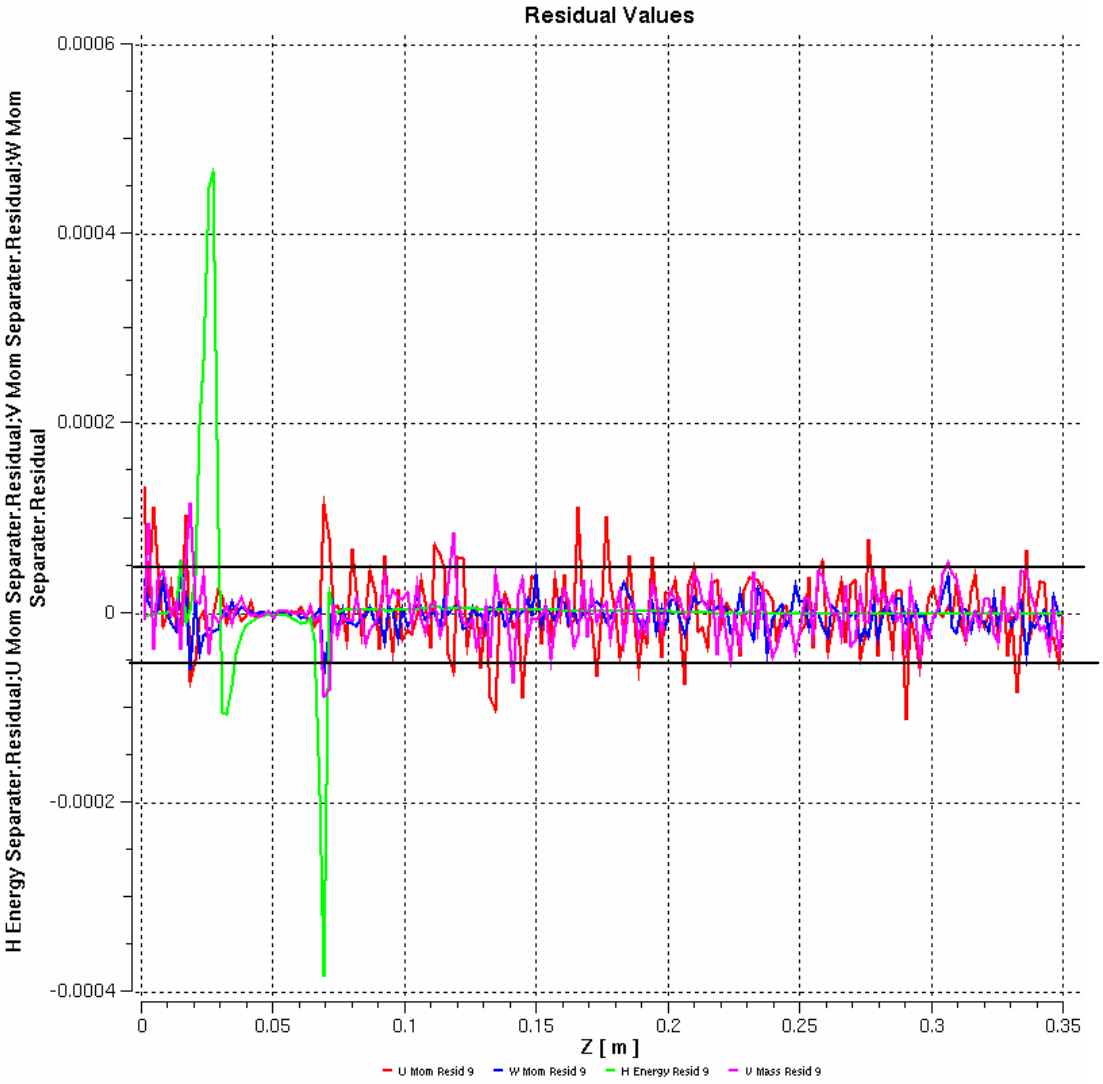

Figure 13 Residual Values for "u" (red), "v" (purple), "w" (blue), and Energy (green). The black lines are at values of 5e-5 and -5e-5. Residual values between the black lines are considered a converged solution.

The most obvious issue from this plot is that the solver is having difficulty achieving convergence in the energy equation at the needle injection inlet (z = .027 meters), and then again for at a z value of approximately z = .07 meters. A comparison of these longitudinal positions with Figure 10 indicates that the energy residual is strongly impacted by the Reynolds number regime, and more importantly the *transition* from one regime to another creates difficulties for the solver. In the lower region of the separation vessel (from z = 0.1 to 0.402 meters), the energy equation is achieving good convergence.

For the velocity values, particular points of interest do not stand out, but rather the residual error is beyond convergence values along the much of the length. The residual values for the velocity components are obviously lower near the inlet region, from approximately z = 0.03 to z = 0.07 meters. But these residual values only represent the centerline of the reaction vessel. In order to see if this holds true throughout the vessel, consideration of residual values at various radial locations is necessary. Figure 14 shows the radial positions considered for z = 0 to z = 0.4 meters.

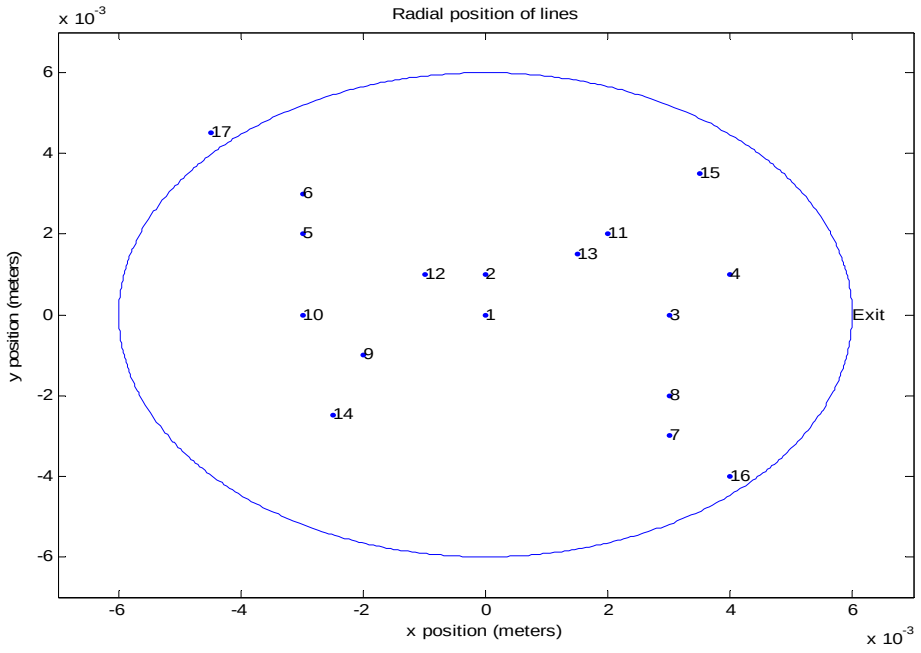

Figure 14 Radial Position of Residual Value Plots

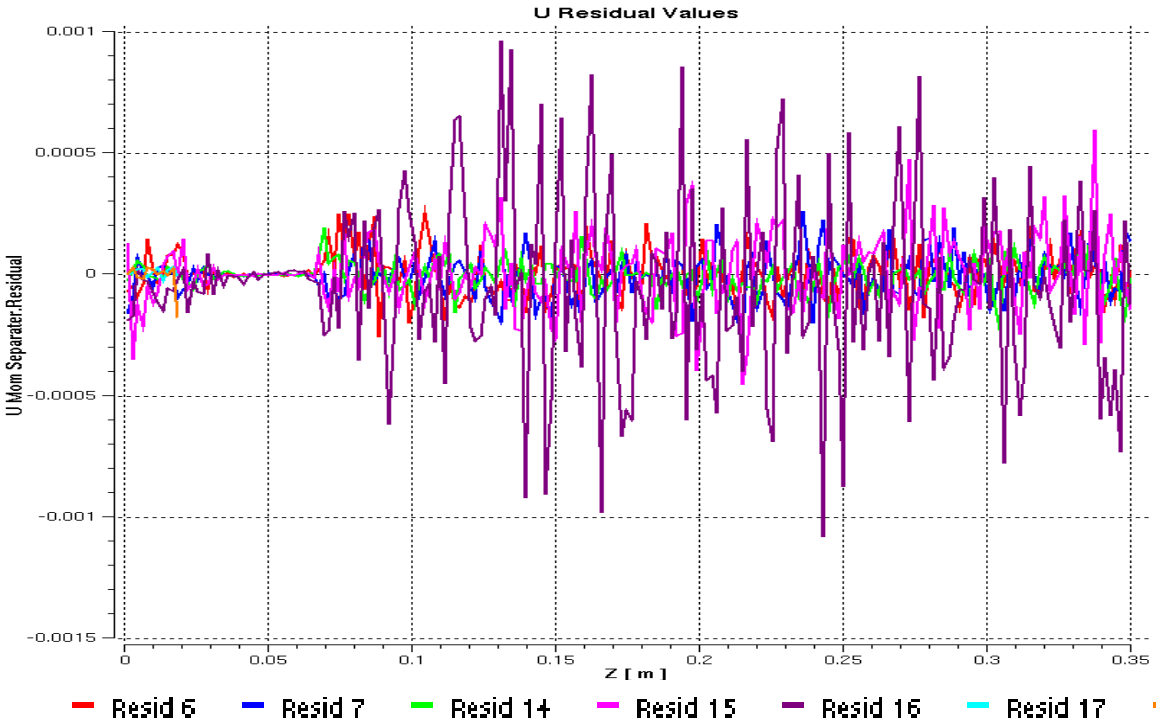

Figure 15 "u" Residual Values at Various Radial Positions

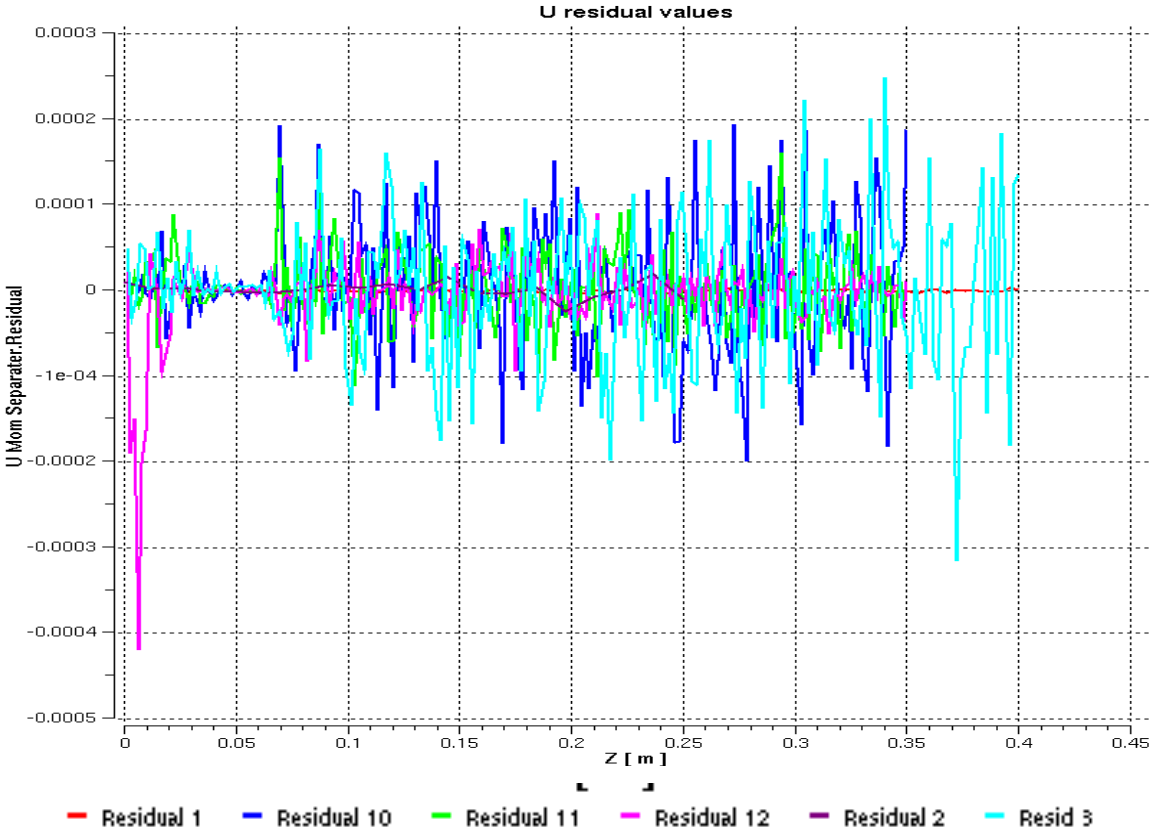

Figure 16 "u" Residual Values at Various Radial Positions

Figures 15 and 16 give the residuals for the radial positions shown in Figure 14. The large residual for radial position 12 from z=0 to z=0.02 is most likely because of its position. Radial position 12 is in the boundary layer of the needle injection tube, where the mesh spacing is not nearly fine enough to capture the rapidly changing velocity properties. Mesh spacing for the boundary regions could be accomplished only for the outer wall boundary and not also for the injection tube. The inability to finely discretize this boundary region impacts the results.

All radial positions show good convergence from the injection needle inlet to approximately 0.07 meters. This indicates that the bulk properties of the flow in this region are relatively constant. The higher residuals for values of z between 0.07 and 0.4 meters indicate that bulk flow properties do not have constant values over time. This could be due to re-circulation of fluid or small eddies on lengths scales smaller than the mesh spacing. The rapid change in residual error for all radial positions near z=0.07 meters indicates that a physical property of the flow changes at 0.07. Referring back to Figure 10 (Reynolds numbers as function of length along the vessel) shows that the Reynolds number decreases into the transitional and laminar regime near z = 0.07 meters. As discovered earlier, the change from one flow regime to another has a strong impact on the results of the numerical solution.

Having looked at aggregate residual value results and element residual results at various locations in the separation vessel, it is somewhat clearer why the solver has not returned a converged solution. The results indicate that rapid and large changes in Reynolds Number, due to combined changes in velocity and temperature, impact the convergence. The results presented so far also encourage a more thorough investigation of the region near in the inlet injection tube. Figure 16 presents the velocity contour and temperature contour for mesh 3 using the standard k-epsilon turbulence model.

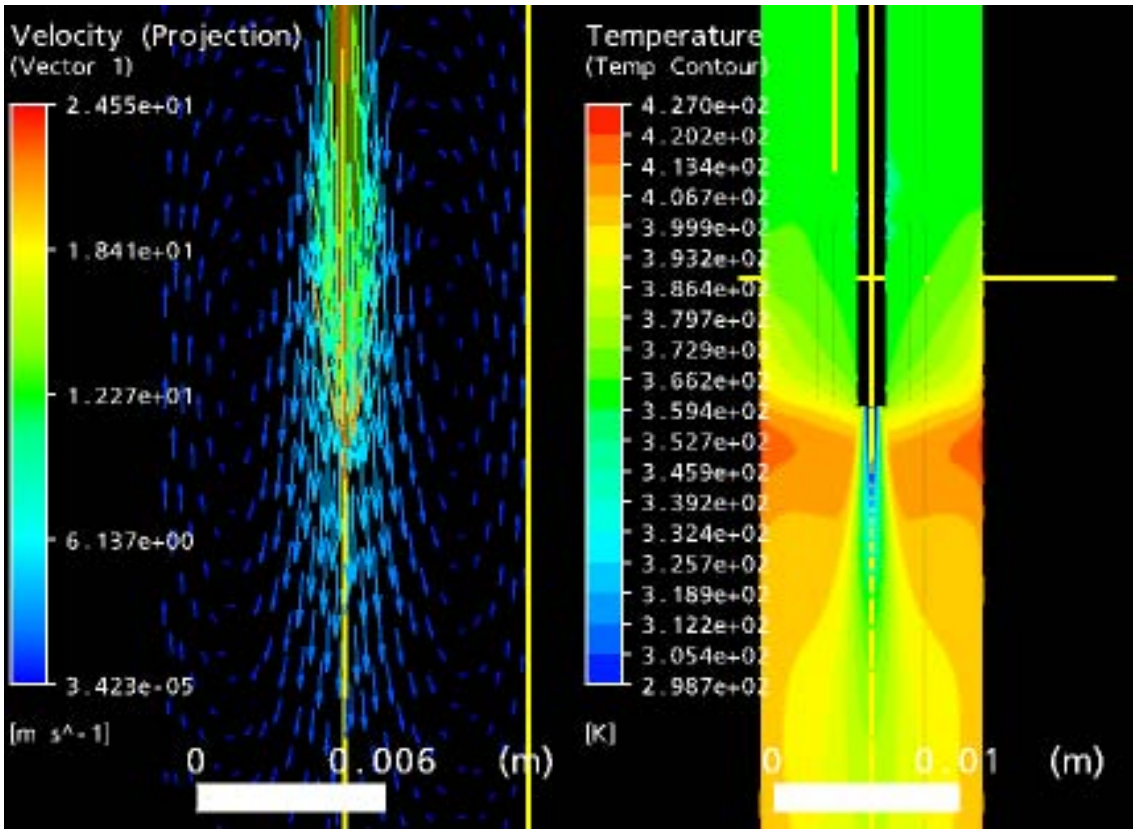

Figure 17 Velocity Vectors and Temperature Contours near Injection Needle Inlet (note different scales on each plot). Velocity magnitudes range from approximately zero (dark blue) to 2.45 m/s (red). Temperatures range from 298 K (dark blue) to 427 K (red). In both cases, changes in color represent changes in variable magnitude.

The plots show that strong temperature gradients exist near the needle injection inlet and extend down the tube for about 10 mm. Not surprisingly, the velocity vectors on the left show that recirculation occurs within the same region as the strong temperature gradient. Based on these two observations, an analysis of the flow properties from z = 0.027 meters to z = 0.04 meters follows.

5.2.1 Flow Analysis: z = 0.027 to 0.04 meters

Starting again with Reynolds numbers, Figure 17 shows the calculated values for four different radial positions.

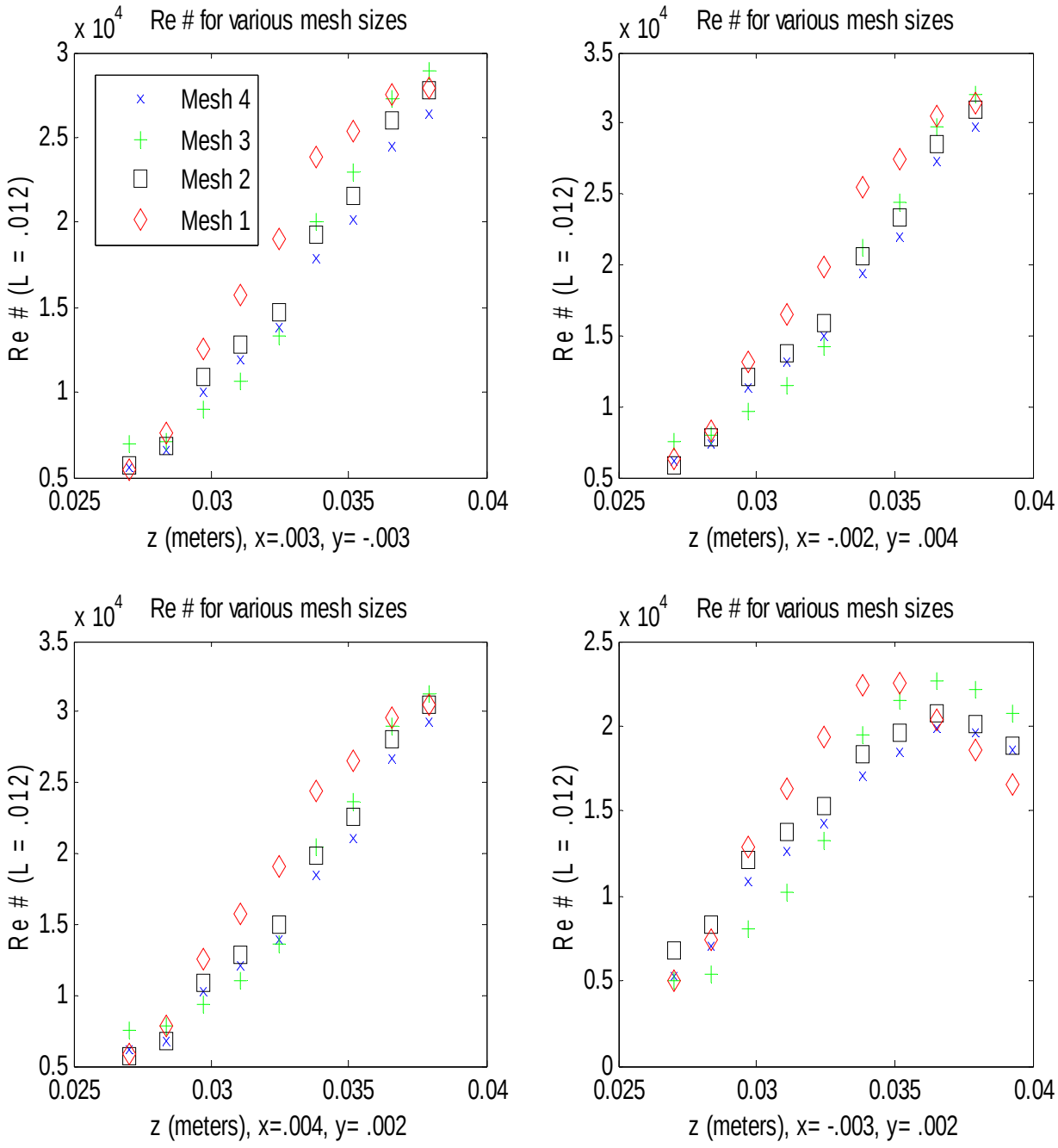

Figure 18 Reynolds Number at Region of Inlet, Various x and y Locations

Figure 18 is helpful when discussing the validity of solutions near the inlet. The Reynolds number near the injection needle inlet (z = 0.027 m) is above 4000, indicating that flow is turbulent in this region. Intuitively, it makes sense that near the inlet, the velocities will be higher and therefore the flow is turbulent. Interestingly, the Reynolds numbers show variation not just in value but in gradient from one radial position to another. Why, though, is the gradient different? First it must be confirmed that the difference in gradient is not due to an issue with the solver, i.e. poor convergence at the radial position (x= -0.003, y= 0.002) while good radial convergence at the other three radial positions was observed.

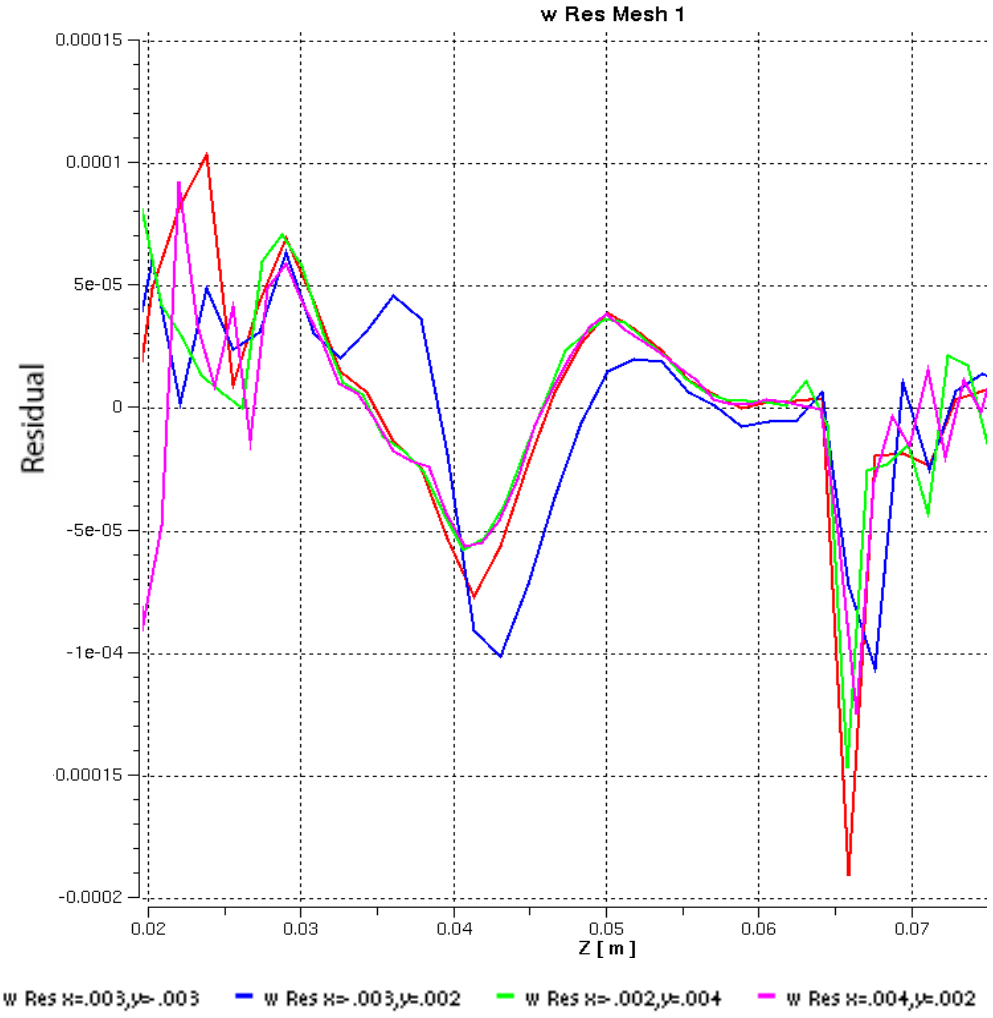

Figure 19 Residual Values at Four Radial Positions for "w" Velocity, as calculated for the momentum equation in the "w" direction

Figure 19 shows that the value of the residual within the region of interest is not substantially larger than the residuals for the other three radial positions and therefore the

Reynolds number trends shown in Figure 18 can be assumed accurate. If those are accurate, what causes the difference in Reynolds Number at that radial position? A review of the temperature and density values show that they are not much different at the four radial positions and do not show the same gradient difference as seen in Figure 18. A review of the velocity values, however, does show similar gradient differences. Figure 20 shows the velocity magnitude at the four radial positions.

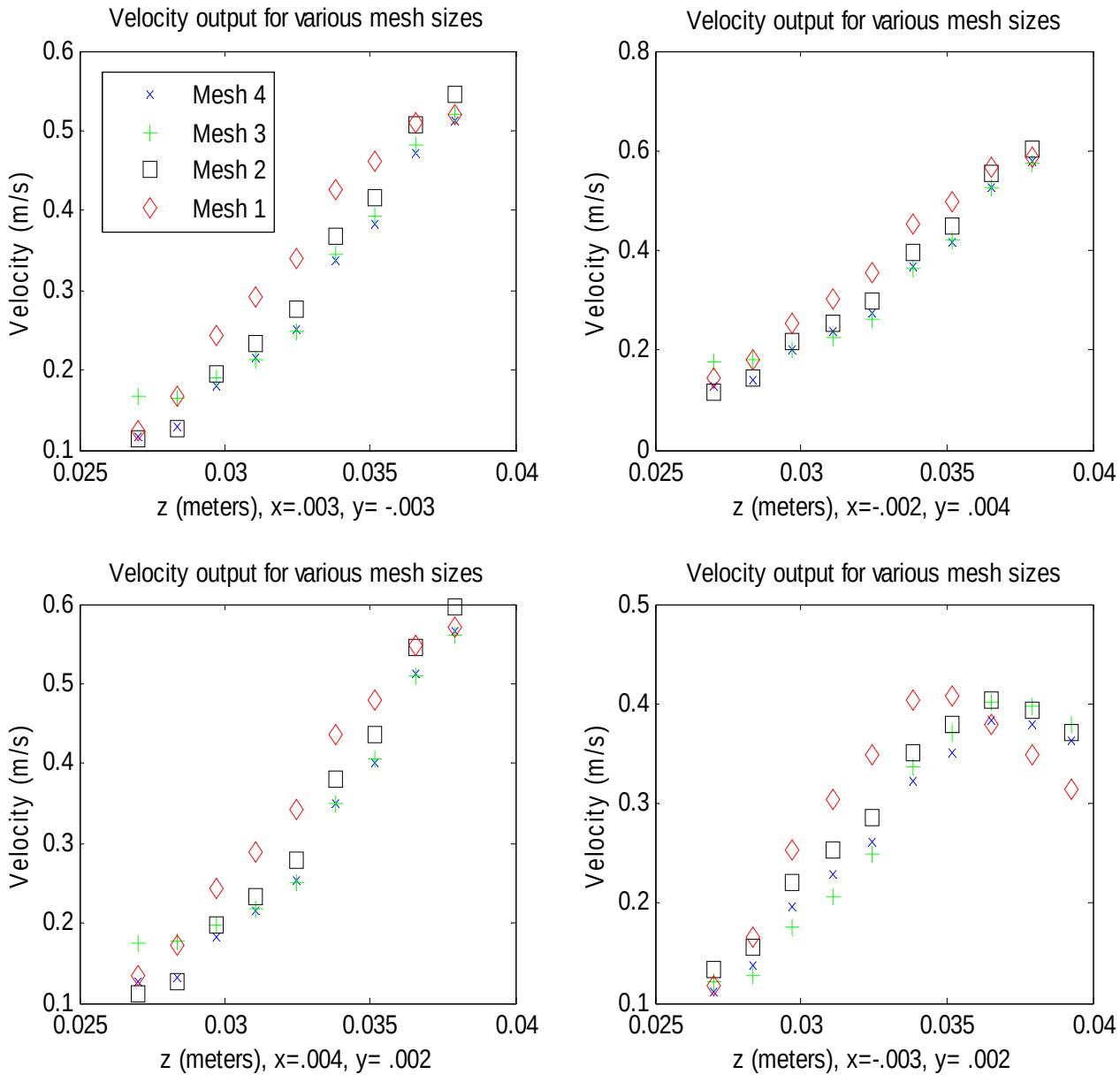

Figure 20 Velocity Magnitude at Various Radial Locations

No matter what mesh was used, simulation results indicate that the velocity is increasing for radial locations in the first three plots but decreasing in the radial location shown in the final plot. This observation can possibly be helpful in understanding recirculation or flow reversal near the fluid inlet, though it must be emphasized that these radial locations are not necessarily streamlines, and therefore one fluid particle will not track in time with the plotted velocities. An inspection of the individual directional velocities (u,v,w) is helpful for this. Reviewing the "u" and "v" velocity plots does not yield much information, but the "w" velocity results are interesting. Figure 20 shows velocity magnitude in the "w" direction.

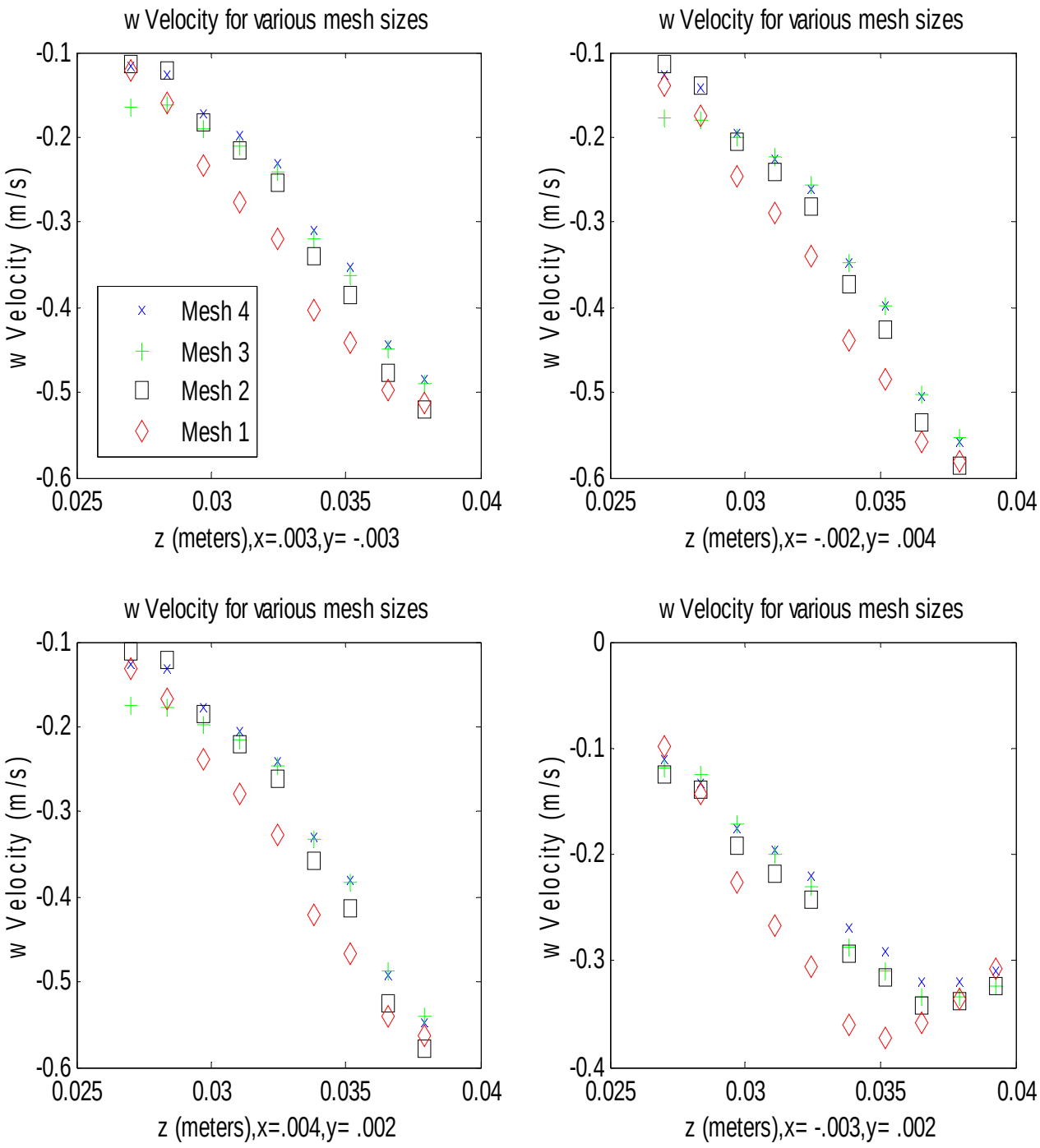

Figure 21 "w" Velocity Magnitude at Various Radial Locations

Again, the gradient is present at the fourth radial position. But interestingly, the velocity at all four radial positions is in the upward direction. The results indicate that at a radial

position where x or y is greater than .002 mm, buoyancy forces have overcome the gravitational force and the flow is reversed. The temperature contour in Figure 17 also shows a steep gradient inside a 2 mm radius of the cylinder center, though this is more of a qualitative observation.

The results presented above point to a small region near the flow entrance to the separation vessel where much of the flow and temperature changes occur for the given simulation boundary conditions. More importantly, the results show the impact of different flow regimes and indicate that a transitional flow regime has a strong impact on the convergence of both the momentum and energy equations.

5.3 Turbulence Model Analysis

Various turbulence models were run for mesh 3 and a comparison of the results gives greater insight into their impact on simulation results.

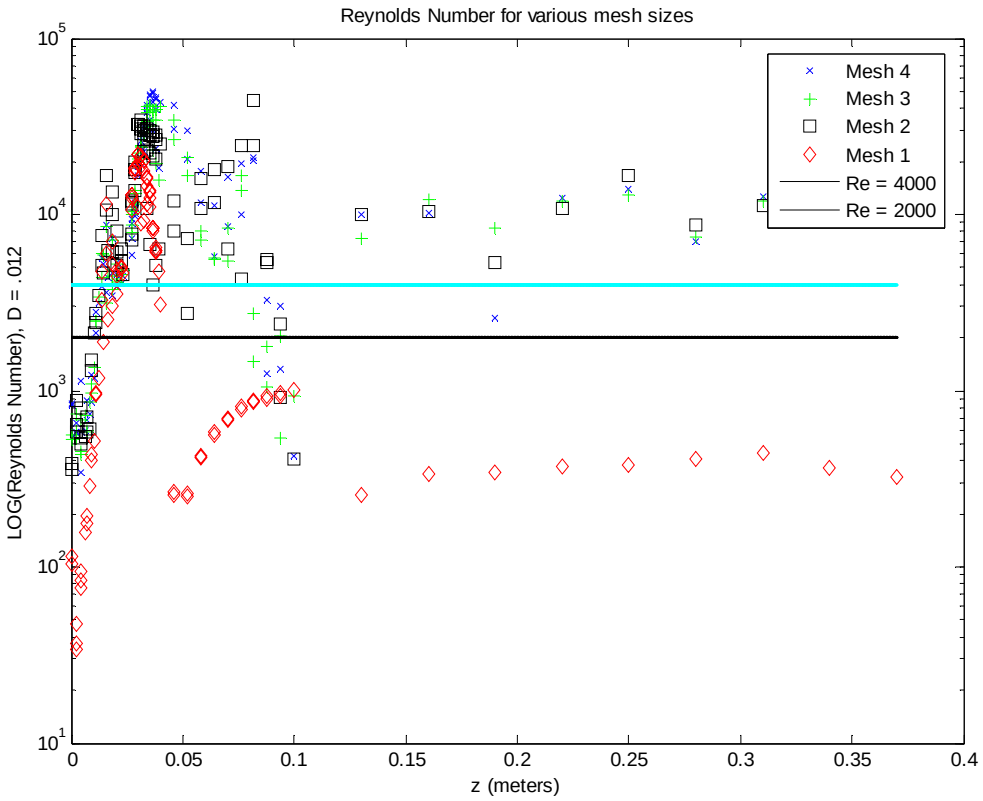

Figure 22 Reynolds number calculated using various Turbulence Models

The blue stars mark the Reynolds number for the standard k-epsilon turbulence model which was used to compare the different mesh sizes in section 5.1. Interestingly, four of the remaining five turbulence models predict Reynolds numbers clearly in the turbulent regime for the length of the separation vessel. Whether or not this will impact the convergence of the solution in those regions is of interest, as convergence issues in the region of fluid flow regime change were encountered previously. The aggregate residuals for the five tested turbulence models are shown in Table 8.

Results for BSL turbulence model				Results for SST turbulence model		
	Distance	PeakRes	FinalResid	Distance	PeakRes	FinalResid
"u" momentum	0.372047	2.10E-03	4.78E-04	0.192891	2.32E-03	5.46E-04
"v" momentum	0.355549	2.08E-03	4.77E-04	0.069254	2.32E-03	5.42E-04
"w" momentum	0.007437	2.80E-03	1.71E-04	0.011759	2.89E-03	2.02E-04
Energy Equation	0.3668	6.55E-03	1.21E-03	0.375	1.08E-02	1.17E-03
Results for k-epsilon turbulence model				Results for Eddy Viscosity turbulence model		
	Distance	PeakRes	FinalResid	Distance	PeakRes	FinalResid
"u" momentum	0.305357	9.67E-04	2.38E-04	0.37501	2.19E-03	4.79E-04
"v" momentum	0.202587	9.35E-04	2.41E-04	0.229576	2.18E-03	4.75E-04
"w" momentum	0.011051	6.39E-04	7.96E-05	0.264018	2.26E-03	1.75E-04
Energy Equation	0.375	1.31E-03	2.09E-04	0.375	7.22E-03	1.59E-03
Results for k-omega turbulence model						
	Distance	PeakRes	FinalResid			
"u" momentum	0.339809	2.01E-03	5.49E-04			
"v" momentum	0.306819	1.99E-03	5.45E-04			
"w" momentum	0.302317	3.20E-03	2.15E-04			
Energy Equation	0.2985	1.04E-02	1.93E-03			

Table 8 Residual Values of Concern for Various Turbulence Models. "Distance" is defined as the distance from the needle injection point to the maximum residual value. "PeakRes" and "Final Resid" are defined in footnotes 2 and 3, respectively.

The results shown in Figure 22 and Table 8 suggest that there is not substantial difference in the overall residual values for the different turbulence models. Although each model is resulting in a solution of equal convergence, the Reynolds number plot shows that there is considerable difference in the actual numerical results found for velocity values for each turbulence model. For example, Figure 23 shows the calculated temperature as a function of length for the injection needle inlet region.

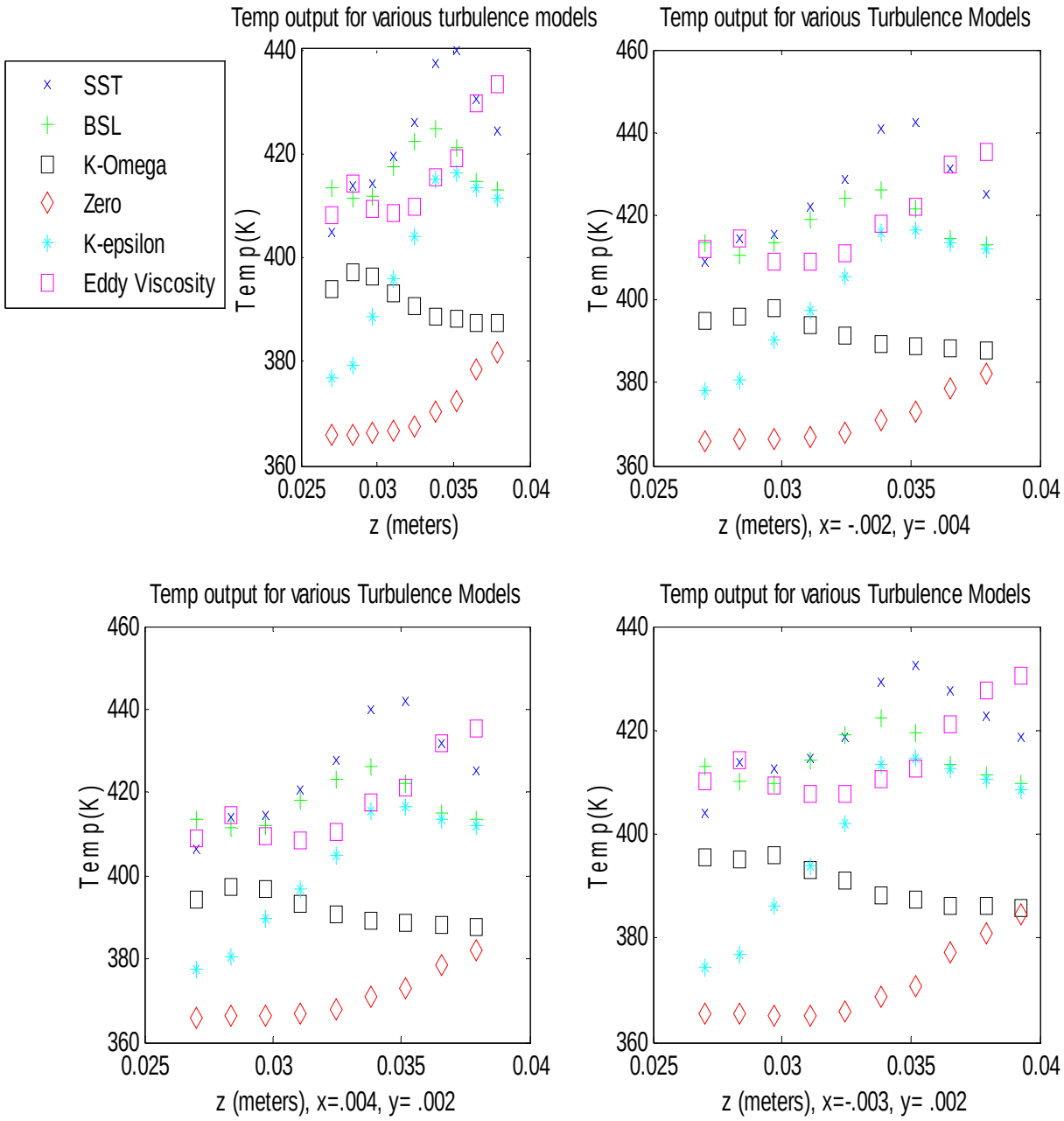

Figure 23 Temperature Results for Various Turbulence Models

These results are clearly not reassuring. For the high mass flow rate of 1000 mL/min (0.01666 kg/s), which results in vessel flow velocities on the order of 10 m/s, there is considerable difference in results from one turbulence model to another. The simulated variation in temperature is as much 40 K (excluding the first order Zero equation

turbulence model) at any one solution point. The task of selecting one of these turbulence models to represent the salt separation process is in no way trivial. Figure 24 is included to provide a comparison between turbulence model sensitivity and meshing sensitivity.

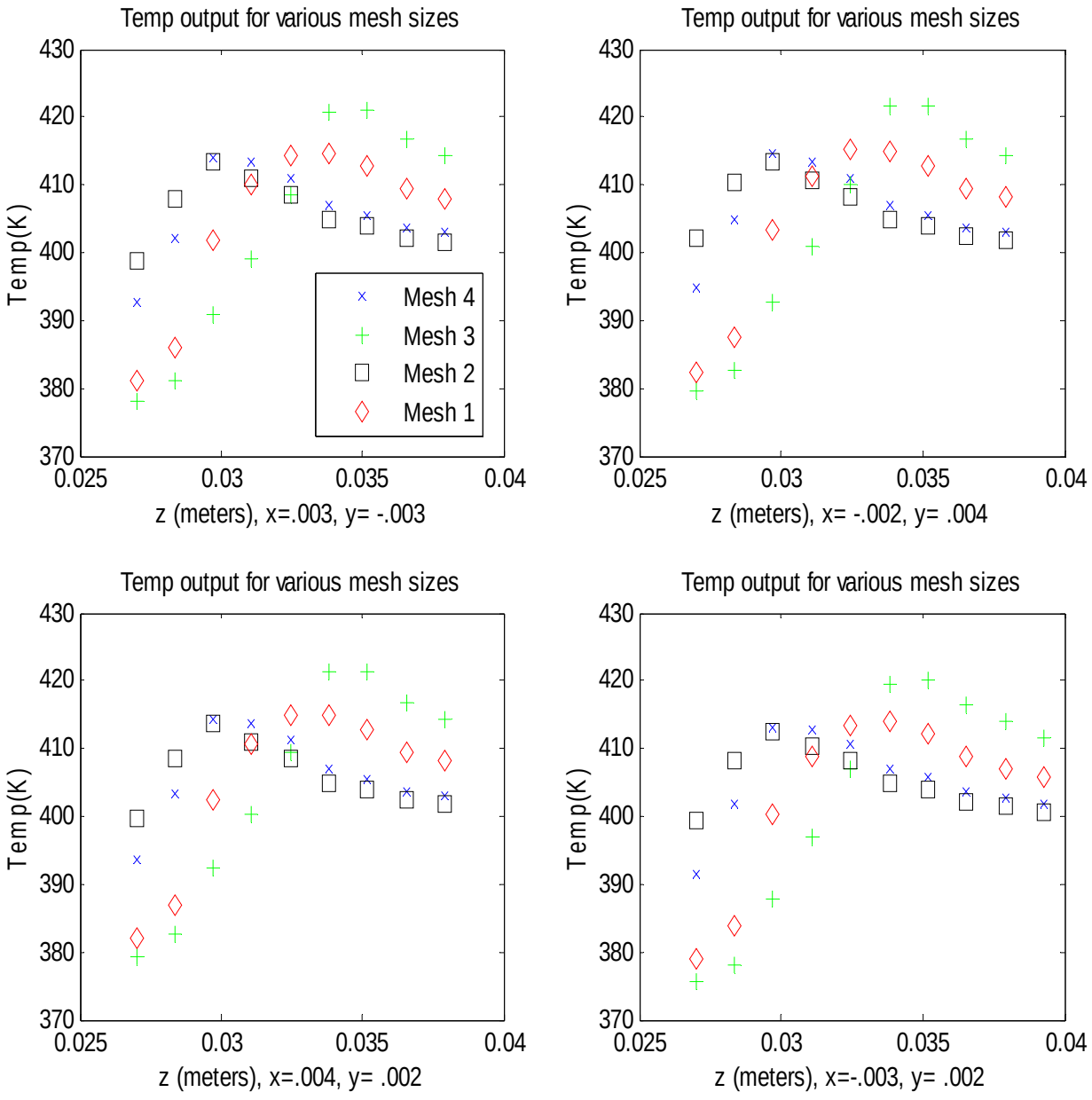

Figure 24 Temperature Results at Various Mesh Refinements

From these results, the spread in calculated temperature looks to be no more than 25 K, indicating that results are impacted more by turbulence models than by mesh refinement.

This is not good. Estimating error based on meshing results (though not performed here due to computational limitations) is possible, but estimating error for a turbulence model is not possible. So, not only will turbulence models provide wide variation in results, but methods to analyze those variations are not currently available.

It is worth looking at velocity results, also, as the turbulence models may have less variation in solving for these variables. Figures 25 and 26 are both Velocity Results, 25 for different turbulence models and 26 for various meshing refinements. Again, the calculated velocity values indicate that there are greater variations from the choice of turbulence models then there are for the various meshing refinements.

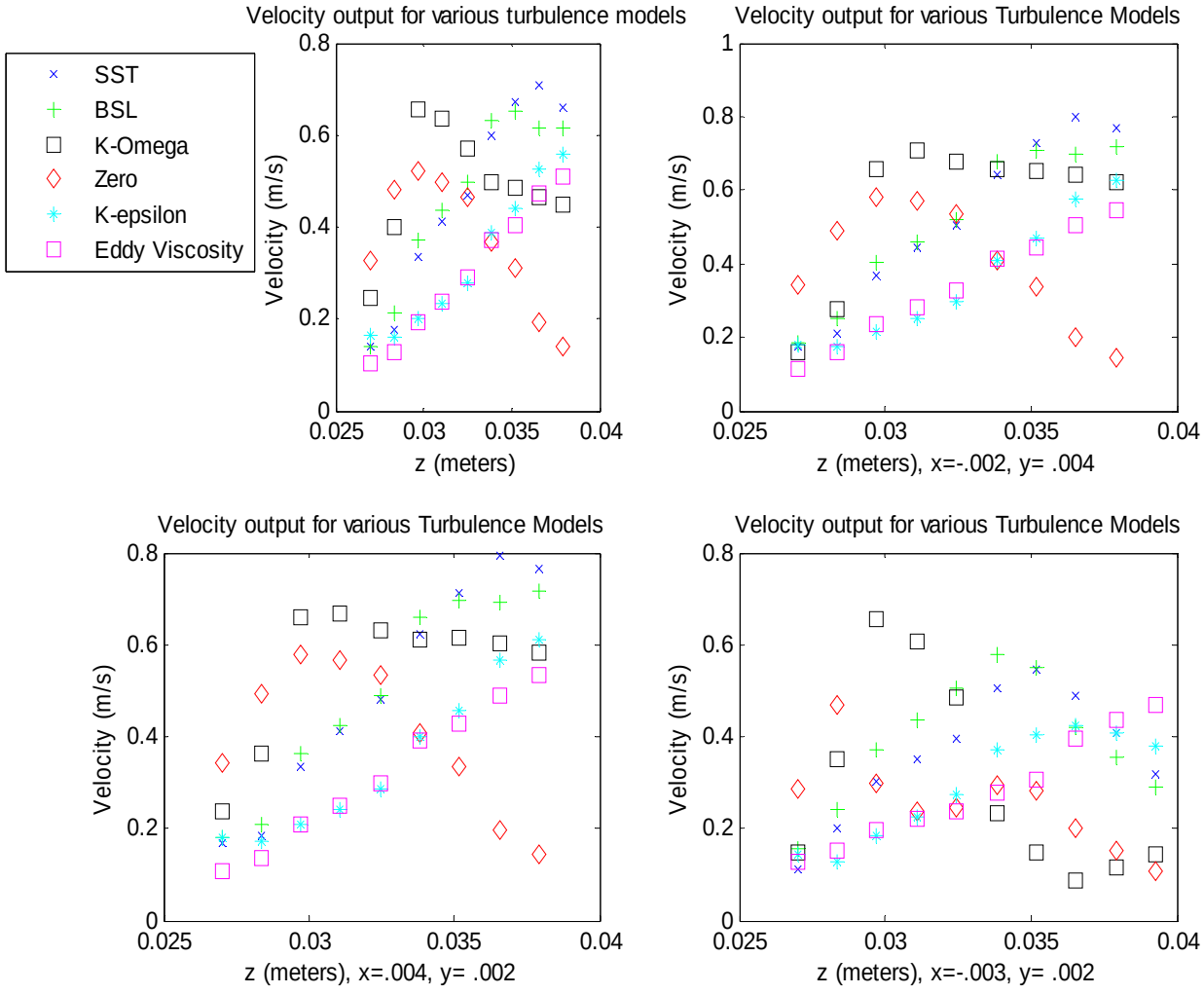

Figure 25 Velocity Output for Various Turbulence Models

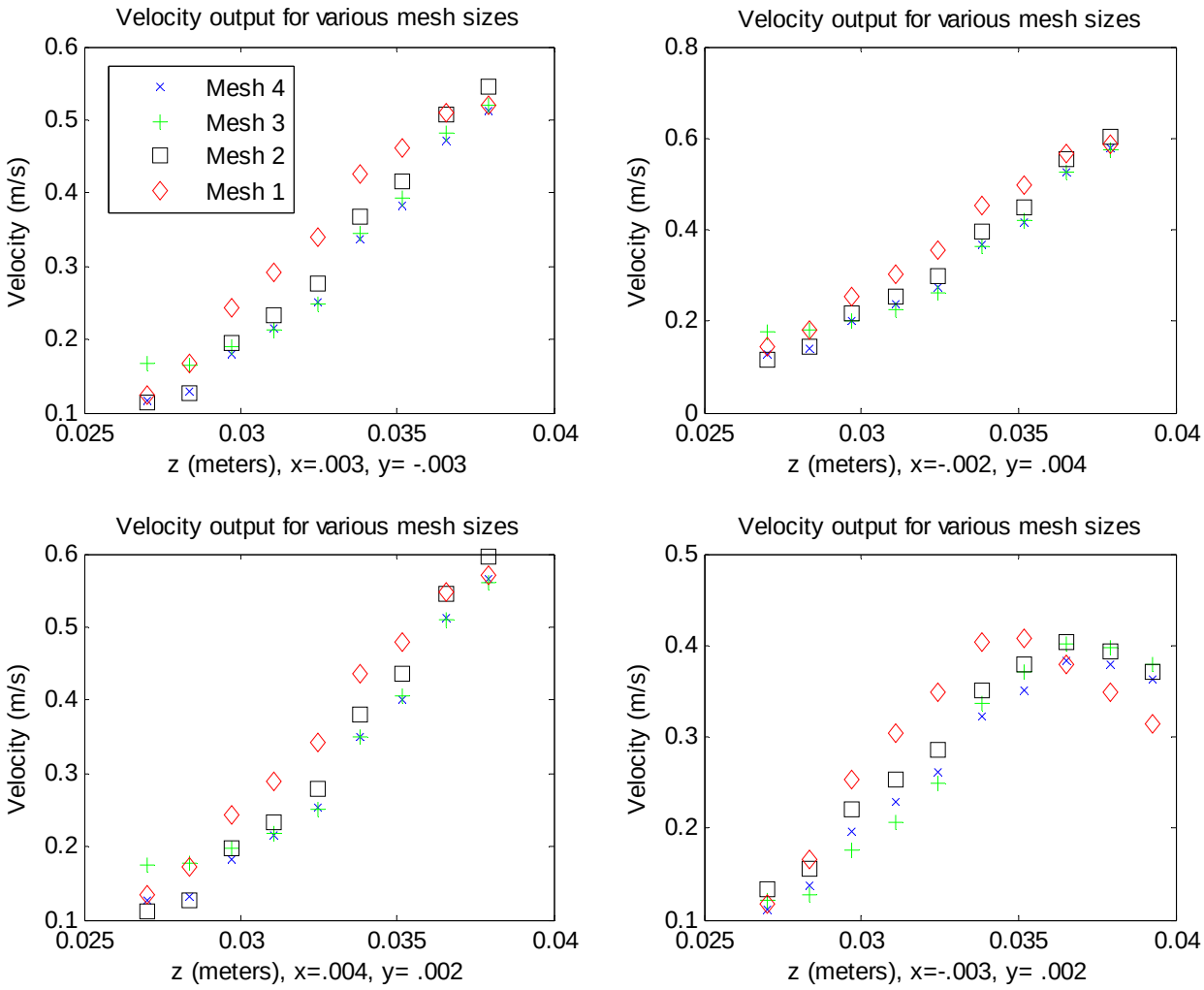

Figure 26 Velocity Results at Various Mesh Refinements

5.4 One Comparison to Empirical Data

Though the results of the numerical simulations using a 1000 ml/min mass flow rate are not converged, it is still worth looking at the results of a 10 ml/min mass flow rate and comparing those results to empirical data. For this simulation, the standard k-epsilon turbulence model, with the finest mesh refinement, Mesh 1, is used to generate results.

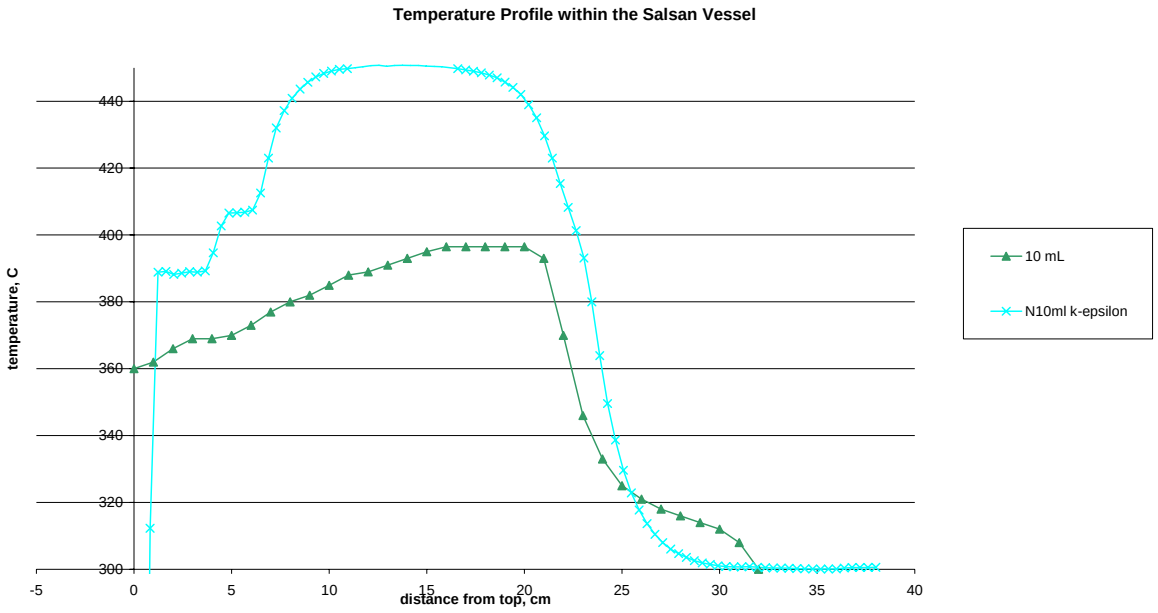

Figure 27 Numerical results for fluid temperature in °C, Compared to empirical results, 10 mL/min

The results shown in Figure 27 indicate that the numerical simulation only indicates trends in temperature profile during operation of the salt separator. Quantitative agreement clearly was not obtained and would necessitate further refinements of the mesh and the use of a validated statistical turbulence model. Considerable mesh refinement is needed to even consider additional tests at mass flow rate of 10 mL/min.

6. Liquid Waste Water Disposal for US Navy Ships

After considering the numerical analysis presented in chapters 2 through 5, it is worth examining an area where super critical water, along with other unique physical, chemical, and biological processes, are currently in use. Numerous studies have been performed to determine the impact of shipboard waste discharge (whether it be human or food wastes, support waste, or machinery waste) on the ocean environment [18, 22]. Although the ocean is vast and voluminous, there are environmental impacts from the introduction of alien and harmful wastes into local ecosystems. The negative impacts have been recognized and both international and local laws regulate acceptable discharges in many parts of the world's oceans, particularly within close distance to the coast and in ports. As the legal discharge requirements become more stringent, there must be an accompanying change in disposal technology. Ships are limited by their size in what they can possibly hold onboard and often times limited by their schedule as to how often they can offload their generated waste.

Processing of shipboard waste, whether it is total destruction of the waste or separation of the harmful waste stream from the benign constituents, is essential to ensuring the longtime stability of the world's water ecosystems. There are numerous companies and agencies investigating the implementation of unique chemical and physical processes, including hydrothermal (high temperature and high pressure processes), in the destruction of shipboard waste. In addition, such treatment may permit recycling of fresh water for shipboard use. These new technologies present an opportunity to positively impact the environment and possibly improve the cost of operating ships in terms of their energy efficiency and environmental sustainability.

The U.S. Navy spent an estimated $54 million[6] on surface ship and submarine waste water disposal in fiscal year 2006. Additionally, international and federal regulations continue to tighten overboard discharge requirements for many of the globe's

[6] Value provided by NAVSEA Environmental Systems division. Represents money paid for disposal in foreign and U.S. ports for all USN ships.

navigable waters. The Navy has long followed environmental regulations, which tend to be extremely stringent in the littoral region (for example, within 3 miles of land no discharging overboard of black water, and within 25 miles of land no discharging overboard of oily waste (at levels of certain ppm's)) and much less stringent in blue-water regions (for example, discharging oily waste when outside of 50 nautical miles of land). As the need to operate in the littorals increases, the ability to reliably process large flow rates of organic wastes will also increase. Waste water treatment systems which can be successfully installed and operated on US Navy ships have the possibility of both positive economic and operational impacts. A review of available technologies, with estimates for life cycle waste water disposal, will assist ship designers as they consider waste water treatment systems for shipboard installation.

From an operational perspective, as the operational space for naval ships has continually expanded from the traditional blue-water region to the coastal littoral regions, waste processing, storage, and disposal has increased in importance. When operating in the littoral regions, USN Navy ships must be able to efficiently process shipboard waste and maintain it onboard for long periods of time in order to remain within environmental limitations and without disrupting operational functions.

6.1 Need for Shipboard Waste Disposal

The need for shipboard liquid waste treatment is driven primarily by new local, national, and international laws and regulations which codify the need for environmental responsibility. The impact of unrestricted discharge was acknowledged as far back as 1977 when the Federal Clean Water Act banned untreated sewage discharge in navigable restricted waterways [3]. More recently, MARPOOL (International Maritime Convention for the Prevention of Pollution from Ships) regulations, and United States' federal and state laws have further constrained the discharge allowances for gray water (water produced from "hotel" services, i.e. kitchen, laundry, scullery, etc.) black water (sewage), and oily waste (machinery room waste) liquids.

In addition to the myriad of regulations driving waste water treatment improvements, there are also economic incentives for self sufficient waste water treatment systems onboard US Navy ships. In particular, US Navy ships pay a high cost for shipboard waste removal when in foreign ports. These fees cover the removal, transportation, and destruction of shipboard liquid wastes, and can be very large. As an example, the rate for sewage waste removal in the port of Trieste, Italy is 36 U.S. dollars per cubic meter [38]. For an aircraft carrier size ship, this can easily translate into a cost of $7200 (200 cubic meters of waste) during a single two day port visit. The result over the life of an aircraft carrier (built for a lifecycle of 40 years, and many times operated for 50 years) can conservatively exceed $1 million for sewage waste disposal *while in foreign liberty ports only*. The total liquid waste disposal cost for a ship of this size for its entire life cycle (in homeport, foreign port, and other US ports) can be estimated using a simple cost model (presented in section 6.4) near $50 million. If a reliable waste destruction system can be installed and operated near this cost, then not only has money been saved but US Navy ships become less dependent on host nations. The combined effect of cost savings, increased independence, and environmental improvement is adequate to encourage a thorough review of available treatment processes.

6.2 Current Status of Shipboard Liquid Waste Treatment Designs

There exist different liquid waste treatment processes that have been recently implemented in shipboard environments. The latest technologies have been installed on merchant ships but have yet to be installed on US Navy ships. The reasons for the lag are many and are addressed in [4], [7], [14], [18]. The primary reason why new liquid waste technologies have been installed and operated on merchant ships but not US Navy ships is because of the more stringent design requirements for equipment installed on a warship: space requirements, reliability, maintainability, shock resistance, electromagnetic interference requirements, etc. are all much more important for a Naval vessel than a merchant ship. These more strict design requirements have led many to argue that comparisons between merchant vessel liquid waste treatment and naval vessel liquid waste treatment are not valid. Although this may be true as a generality, if one

chooses comparable ships (size, personnel, flow rates, etc.) and comparisons are done thoughtfully with an understanding of all assumptions, then a comparison is possible.

6.2.1 Current technologies

Technologies for treating liquid wastes are many and vary in their treatment technique. Some utilize physical processes, others chemical treatment, other biological treatments, and still others use a combination of processes. Processes which have been installed, or show promise for future use, are listed in Table 9.

Technology	**Developer**	**Current Users**	**Pros**	**Cons**
Vacuum Collection, Holding and Transfer sytems	Evac Oy, etc. Various	Numerous, to include both merchant and naval vessels	Can hold up to ten times more black water than traditional CHT systems in the same size tanks by reducing volume through reduction in pressure; Can be combined with biological treatment plants for onboard treatment; Simple and proven systems	Without biological treatment capability, the system only reduces required storage volume (or increases days' holding capacity) Biological treatment systems; Require continuous operation; de-sludging necessary on regular basis. Long residence times.
Membrane systems	Various	Celebrity Cruises *Mercury* and *Galaxy*	Proven reliability; Extremely ambitious call to use system to treat all gray and black water onboard so that it can be recycled for use	Membrane plugging, membrane damage is not unheard of. Can be maintenance intensive. Redundancy is necessary.
Batch SCWO technologies	Sandia National Lab	None as of yet	Simplicity of operation, destruction of "unpumpable" solutions, can handle a variety of different wastes, scalable	Batch system, small volume, low flow rates
Biological systems	Multiple, Hamworth		Used in conjunction with	Require continuous

			many other types of systems.	operation; de-sludging necessary on regular basis. Long residence times.
Physical-Chemical treatment	Envirovac, etc.		Simple design of physical separation followed by chlorine treatment	Limited containment capability (if no offload barge, problems). Necessary to store large amounts of caustic chemicals for treatment process
Electrocatalytic Oxidation	Exceltec, etc.	Princess Cruise Lines, Royal Caribbean Cruise Lines	Small footprint, short residence time	High levels of chlorine treatment which may affect overboard discharge;
Plasma Arc Waste Destruction (High temperature process)	Pyrogenesis		Quick start up time, small size, designed specifically with USN in mind	Proven performance with liquid wastes is limited???
Membrane Bioreactor	Naval Sea Systems Command Carderock	USS BONHOMME RICHARD (LHD 6)	Long term test on US Navy ship completed	Volumetric footprint
Supercritical Water Oxidation	General Atomics		Complete organic destruction, able to process many different types of inputs	Large installation footprint, unresolved corrosion issues, flow rate limits to hazardous waste destruction

Table 9 Shipboard Waste Disposal Technologies [1,11,28,30,34]

These technologies vary in terms of volumetric footprint, ease of operation and maintainability, maximum flow rates, and energy efficiency. In order to be considered for use in a shipboard environment, the technology must first meet the flow rates presented in section 6.2.2 and volumetric footprint requirements for various ship classes.

6.2.2 Comparison of Alternatives

In order to fairly compare the performance of a commercially installed waste water treatment system to the needs of a US Navy surface ship, it is important to consider the reliability, availability, and flow rate values that are necessary to meet US Navy

specifications. The Navy design criteria for black and gray water production rates are set at 33 gallons per person, per day onboard a Navy ship (30 gallons gray water, 3 gallons black water). Amazingly, this can amount to 350,000 gallons per day for an aircraft carrier [3]. Any treatment system, regardless the size of the ship, must be capable of treating the individual daily flow rates. For this reason, a size-wise comparison (by tonnage) is not the best method for comparison. Consider that many merchant vessels are built for long open sea transit with minimal crew manning. Oil tankers and cargo carriers, both ships which are equal in size to Navy ships, are in this category. These ships are large, meaning adequate space for waste treatment plant installation, but minimally manned translating to low flow rates of waste production. The systems installed on these types of ships will not translate well to Naval Vessels. If one considers the manning on a 9000 ton guided missile destroyer near 340 personnel and the manning on a 800 foot cargo ship which may have manning levels as low as 20 or 30, it can be estimated that Naval vessel manning is normally at least an order of magnitude greater than tankers. If, however, cruise ships, large vessels carrying large numbers of passengers, are compared to aircraft carriers, another large ship with comparable passengers, then technologies can be evaluated and considered for cross-decking. To state it more directly, if it works on a cruise ship, it stands a high probability of working on an aircraft carrier (with some modifications, of course).

The two most difficult requirements for waste water treatment plants to meet for USN ships are the daily flow rates and the space requirements. Using the Navy's daily flow rate estimates (30 gallons per person, per day for gray water and 3 gallons per person, per day for black water), the flow rates necessary for different classes of current ships are shown in Table 10.

Ship	Max Personnel	Flow Rates (gal/day)		Flow rates (lb/hr)		Flow rates (liter/hr)	
		Grey Water	Black Water	Grey Water	Black Water	Grey Water	Black Water
Aircraft Carrier	5700	171000	17100	59280	5928	27075	2707.5
Large Deck Amphibious Ship	2500	75000	7500	26000	2600	11875	1187.5
Surface Combatant	300	9000	900	3120	312	1425	142.5

Table 10 Flow Rates for various class US Navy ships

Current technologies must achieve these flow rates in order to be considered for installation on US Navy ships. Due to flow rate requirements, the larger ships initially look to the more unlikely candidates. However, the available volume on these ships is much greater than on a surface combatant and therefore finding volume for installation will be just as much a determining factor as flow rate capability.

6.3 Applications of Supercritical Water Processes

Since the technical research presented in this thesis has focused on supercritical water processes, it is worth presenting additional information in this particular area. The inclusion of this information is not to show that SCWO, or some other hydrothermal process, is the best process for shipboard liquid waste disposal. It is only to demonstrate the variety of successes and potential for continued use in both the Department of Defense and US Navy.

Various Department of Defense and government agencies have been using or studying supercritical water processes for a number of years. The U.S. Army has been studying Supercritical Water Oxidation as a process for secondary destruction of nerve gas. General Atomics (GA) and the US Army have experience with SCWO to destroy chemical nerve agents in unexpended, stockpiled munitions. Flow rates of 1000 lb/hr with over 6000 hours of operation over the past four to five years (since 2003) have been attained for prototype testing. Although the chemical constituents of the nerve agents are very different than a biomass solution, the GA team encountered similar problems with salt build-up and corrosion which will be an issue if SCWO is used on an organic/inorganic solution similar to black water. The lessons learned, technological advances in corrosion reducing liners, scale up proposals, etc may be applicable and relevant to a SCWO system for shipboard installation. What will not be similar, of course, are the size requirements. The current GA/US Army SCWO endeavor covers multiple buildings with almost unlimited space. An SCWO reactor for shipboard installation will unfortunately have a much smaller space available.

NASA has studied SCWO as an option for waste water treatment/water recycling process for both space shuttles and space stations starting in the 1980's. The U.S. Navy, along with merchant vessel construction companies, has considered supercritical water processes for treatment of sewage and oily waste. In 2005, the Office of Naval Research expressed an interest in producing synthetic fuels at sea. Although initial studies centered on producing synthetic fuels from coal, the Naval Research Advisory Committee states that there must be "long term commitment to manufactured liquid hydrocarbon fuels from domestically abundant feedstocks" [9]. Although production of synthetic natural gas and liquid oils from biomass is in its infancy, it does have potential for helping achieve long term national security goals that can be utilized by the military.

6.3.1 Applications of Supercritical Water Processes in a Shipboard Environment

When considered for implementation on a large scale in U.S. Navy ships, the current state of SCWO and SNG production from biomass technologies are at low Technology Readiness Levels. Therefore, if either process is to be considered for future viability, improvements in the scale of the processes at a minimum must be achieved. If Supercritical Water Oxidation can be developed on an industrial scale, with the ability to process approximately 140 gallons of solution per hour (flow rate of 2.33 gallons per minute), and can be operated in a continuous mode vice batch mode, then this would enable ships operating in the littoral region to forego either 1) breaking environmental regulations and discharging black water overboard due to operational necessity, or 2) transiting from littoral regions of operation in order to discharge black water. This will save both fuel and increase time on station (increasing Operational Availability). In a not too distant future, it may even be possible to process black water in order to produce Synthetic Natural Gas or other fuels for combustion in ship's auxiliary power systems.

6.4 Cost Estimates for Shipboard Liquid Waste Disposal

The US Navy has sponsored and performed various research and development initiatives covering the different varieties of liquid waste disposal technologies that are

currently available. Some of these R&D efforts have yielded results which the Navy deemed sufficiently positive for further study (PAWDS, ongoing), and others yielded results which the Navy deemed not sufficiently positive for further study (such as SCWO for wastewater treatment, completed in the late 1990's). The stress in the above sentence should be on "Navy deemed." In other words, the research conducted by the USN (or for the USN) was used to decide to continue or discontinue research in certain areas. The particular decisions by the USN do not mean that private industry or research institutes have exhausted all resources or even consider these particular technologies to be non-viable for shipboard use. The USN decision to discontinue research may have been based on a low Technology Readiness Level, a decrease in available research funds, or unfavorable data from one particular study. The very important issue is that the financial, regulatory, and technology conditions existing at the time of the study may not have been attractive for deploying SCWO or other waste technologies on USN ships. But, liquid waste disposal systems should not be discounted from inclusion in future warships designs based simply on previous USN research results. The continued research in the private and academic sectors has yielded positive results and improvements and, based only on previous successes, improvements look to be far from exhaustion. As shown in Table 9, there are many technologies which have been successfully installed and operated on merchant and civilian ships. Continued discussion about each of these technologies for implementation in USN ships is necessary.

Each technology mentioned in Table 9 involves a connected set of physical, chemical, and/or biological process which has received research attention in private industry, in academic and research institutes, and in government research centers. After performing a high level review of the research results that are available (public domain information only), it would be imprudent to suggest possible improvements or future initiatives to improve the viability of these systems for shipboard installation alone. As operation of the current commercial liquid waste disposal technologies become more proven and robust, ship designers and engineers will determine if technology has matured sufficiently for successful installation and operation in new USN ships. Aside from technological (flow rate limits, operational availability, installation footprint, reliability,

etc.) issues, what economic factors are considered prior to inclusion in a design? Better said, how can the US Navy know whether a technology is not only feasible for installation but also a cost effective installation. Regulatory constraints can also play a major role in changing the visibility of a particular method - it may be required to meet laws, for example. For a system which will operate over the entire life of the ship (25 years plus), a valid comparison must include the entire life cycle cost of the installation compared to the total life cycle cost for liquid waste disposal. If the USN is to leverage the experienced gain in the merchant and civilian ship industry, and consider slightly modified off the shelf technology, then installation, maintenance, and operation costs can be estimated. The life cycle waste water disposal cost for a ship is a somewhat more difficult number to capture and impacted by different variables. Previous cost estimating for shipboard waste disposal has been performed by the Navy Surface Ship Waste Management Program at the Naval Sea Systems Command in 2001[33]. These cost estimating tools were for all shipboard generated wastes and took into account as many as 59 parameters, of which 17 were determined to be critical. The cost model included waste disposal costs at up to 80 different ports (cost data which receives updating every 3 years) and also used historical ship employment data to determine time spent in various locations and probable costs for future ship classes. Calculated cost information was found to be within 20% of actual, which is very reasonable in the difficult discipline of cost estimation.

Given global events since 2001, with the USN's increased commitments throughout the world, extremely volatile and unpredictable national security issues, and increased deployment lengths, it can be argued that a cost model based on historical ship employment data may not be relevant or at least limited in its application. A model which allows for some manipulation of deployment cycles, underway days, etc. would be needed when considering new ship classes for future unknown employment. Rather than based on historical ship employment data, this type of cost model allows the user to manipulate inputs which impact the liquid waste disposal costs. It is also a much simplified cost model that is based on average liquid waste disposal cost ($/gallon). While the cost model is indeed simplified, ship's employment can be modified to see how

different operational tempos and deployment lengths impact the lifetime liquid waste disposal cost for a ship. Therefore, the goal is to develop a cost estimating tool which can show liquid waste disposal costs (as a function of manning and inport days) that can be used in conjunction with the above mentioned NAVSEA cost model.

The starting point for the cost estimating tool is the value for the cost of liquid waste disposal per gallon. In general, this cost can be considered a function of liquid waste production rates, for which estimates have been well established [22]. A specified value for treating waste can be an input into the model and utilized to determine an average cost of waste disposal per ship per year using different deployment lengths and operational tempos. The liquid waste cost will be a function of the ship's schedule, and for the purposes of the liquid waste disposal discussion, a function of the number of hours that the average crew member is onboard the ship annually, producing liquid waste which must then be disposed of. For liquid waste disposal, ship's underway days will be excluded from the liquid waste disposal cost per person (no monetary cost to USN for liquid waste disposal while underway). The number of underway days, however, is still vitally important in determining the number of inport days per year. The liquid waste disposal cost ($/gallon) is the only historical data point necessary to generate cost estimates in this model. The positive of this is that the model is simple. The negative is that the value must be very precise in order to yield an accurate estimate. Comparison of several years' liquid waste disposal costs, ensuring that the entered value is not an anomaly, would be prudent, but is not necessary for the demonstrative purposes of the cost estimating tool.

An additional thought to consider for the cost model is this: For any one year, when comparing two ships from the same class, it is possible that the cost of liquid waste disposal per gallon may differ by as much as 100% or more (consider two ships: one which went through an overhaul period, a long period of inport time, and one which deployed for 7 months with multiple foreign port visits). However, if one were to compare two ships from the same class over their entire lifecycles (period of 25 to 50 years, depending on the ship class), the liquid waste disposal costs per gallon are likely to

be within very close agreement. This is based not on an individual ship's employment, but rather on the assumption that the USN will efficiently manage resources over long periods of time and those resources (ships) will be equally employed (equal number of deployments, underway days, etc.). This is a reasonable assumption and allows for ships to be grouped by class. Additionally, forward deployed ships will experience different liquid waste disposal costs over the life of the ship, but when ship designers are considering cost estimates for an entire class of ships, there will be limited data about the number of forward deployed ships and how these particular assignments will impact class life cycle cost. Knowing, however, that forward deployed ships make up less than 10% of all ships, leads to the conclusion that decisions using the cost model should be based on the largest percentage of ships, or the 90% that will spend their lifecycle in US homeports.

With the initial input of the waste disposal cost, the other inputs are:

Underway days for training (per deployment), Cost model will also determine if the number of training days cannot be supported due to the short time between deployments an adjusts the number of underway training days

Underway days for Fleet Exercises (per deployment), Cost model will also determine if the number of training days cannot be supported due to the short time between deployments an adjusts the number of underway training days

Foreign Port Factor: Factor which determines the number of foreign port visit days during a deployment. Takes into account that a longer deployment will likely have more foreign port visits

Max Foreign Port Visits: Limits the number of Foreign Port Visit days

Constant Non-homeport visits (per deployment cycle): Number of days normally spent loading/unloading ammunition or receiving technical support

Deployment Lengths: Three different deployment lengths are possible for comparison's sake.

Time between Deployments: Three different non-deployed time lengths are possible for comparison's sake.

These factors can be manipulated by the operator in order to produce different liquid waste water disposal estimates for a class of ships. If a company represents a valid

waste water technology for installation with an estimated acquisition and operating cost, then the cost estimator can be used to determine under what operational scenarios the installation is cost effective.

6.4.1 Sensitivity test of Cost Estimator

The cost estimator provides liquid waste water cost estimates for various employment cycles which are based on two basic time scales: length of deployment and length between deployments. In Table 11, under outputs, the numbers written "X/Y" define the length of deployment and length of time between deployments, in months, respectively. The "Mod Combination" can be manipulated by the user in order to define different employment usage throughout the life a ship, for example a "6/18" employment for 60% of ship's life and an "8/16" employment for 40% of ship's life. This combined cost estimate acknowledges that ship's employment does vary due to national security needs throughout the life of the ship. Table 11 shows cost estimates for three employment variations. Appendix B shows all inputs, outputs, and calculations for the cost estimator.

Inputs:				Outputs			
				6/18	8/12	9/11	Mod Combination
Crew		5700					
Life Cycle		40	Per Ship	46.5	36.3	36.0	41.1
#Ship Class		9	Per Class	418.6	327.0	323.8	370.3
Inputs:				Outputs			
				6/18	8/12	9/11	Mod Combination
Crew		5700					
Life Cycle		50	Per Ship	58.1	45.4	45.0	51.4
#Ship Class		9	Per Class	523.3	408.7	404.7	462.9
Inputs:				Outputs			
				6/18	8/12	9/11	Mod Combination
Crew		2900					
Life Cycle		35	Per Ship	13.1	10.5	10.4	11.6
#Ship Class		7	Per Class	91.4	73.3	72.9	81.5

Inputs:				Outputs			
				6/18	8/12	9/11	Mod Combination
Crew		364					
Life Cycle		35	Per Ship	4.6	3.5	3.5	4.0
#Ship Class		24	Per Class	109.4	84.0	82.8	96.2
Inputs:				Outputs			
				6/18	8/12	9/11	Mod Combination
Crew		364					
Life Cycle		25	Per Ship	3.3	2.5	2.5	2.9
#Ship Class		24	Per Class	78.1	60.0	59.2	68.7

Table 11 Cost Estimates for Various Crew Sizes, Life Cycles

As expected, a sensitivity test shows that a very large ship, with a large number of personnel, provides the greatest opportunity for return on investment when installing waste water treatment systems. Interestingly, though, the cost estimate for a medium size ship, with a low number of ships in the class, is roughly equivalent to a smaller ship with a greater number of ships in the class. This analysis shows that research, development, and initial investment money is best spent on installing liquid waste disposal systems on large aircraft carriers. Once proven on ships of that size, then the benefit from installation on medium size ships and smaller surface combatants is roughly equal.

7. Conclusions and Recommendations for Further Study

7.1 Shipboard Applications

The review and cost model presented here hope to further encourage the US Navy's research into unique processes to treat liquid waste water. Not only do the waste water systems decrease the impact on the environment, but they also improve ship's operational availability and decrease dependence on host nations. In today's globally connected world, the Navy's ability to perform peacetime and training missions is impacted by its presentation in a positive, environmentally sustainable manner. With the increase in environmental consciousness, any efforts to reduce environmental impact are sure to have positive impacts on others opinions. In addition to the positive press impacts on operations and public opinion, there are economic incentives which show that some return on investment is possible. The Navy should continue to leverage relevant commercial technology development and determine which systems in particular have been successful. For example, waste treatment and water recycling options planned for zero-discharge on cruise ships which also carry large numbers of people may be particularly applicable.

7.2 Numerical Simulations

In order to achieve the results and conclusions presented in this report, it was necessary to start with a ground up approach. As a result, all conclusions are based on analysis performed with as much experience that can be gained with hardware, software, meshing properties, turbulence models, and numerical methods in a eleven month period. Research in this area can continue starting with a baseline of knowledge and equipment that was collected in the performance of this study. Specific conclusions of interest are included below.

1. The validity of three-dimensional numerical simulations from a single processor system is difficult to access. Unfortunately, due to memory and processor limitations, mesh refinement is limited. Future studies which consider three-dimensional fluid flow

should be conducted on multi-processor systems with large amounts of accessible memory. This enables the calculation of an error estimate and gives some value to the proposed accuracy of the simulations.

2. Initial testing of the various turbulence models shows a very large variation in results based simply on the mathematical model used to represent unsteady flow.

3. Results from of simulations using the k-epsilon turbulence model show that there is a large dependence on Reynolds Number and that convergence is negatively impacted by transitional regimes. Further testing of the other turbulence models will determine their sensitivity to Reynolds Number.

4. Large variation in the results from different turbulence models will impact the numerical solution. If numerical simulations are used for optimization, additional research is needed into the validity of the turbulence models for the proposed application. Most CFD researchers advise that the best method for choosing a turbulence model is by comparing empirical results to numerical results. A sensitivity analysis of the non-converged solution at 10 mL/min, with different turbulence models, may also provide a means for solution, though it may not yield acceptable results.

5. Any scale up optimization process must be conducted in at least two dimensions, recognizing that results for axi-symmetric simulations will not match exactly the physical conditions inside SALSAN or Konti-2 salt separation vessels.

BIBLIOGRAPHY

1. "Advanced Waste-treatment Solution for Passenger Ships." Naval Architect, Feb. 2006. pp. 50 - 51.

2. Bathe, Klaus-Jurgen. Finite Element Procedures. Prentice Hall, Inc. Upper Saddle River, NJ. 1996.

3. Benson, J. et al. "Blackwater and Graywater on U.S. Navy Ships: Technical Challenges and Solutions." Naval Engineers Journal, May 1999. pp 293 - 305.

4. Brown, S. H., et al. "Integrated Liquid Discharge System for Waste Disposal on Future Surface Combatants." Naval Engineers Journals, May 1999. pp 285 - 291.

5. Cheng, X., et al. "Heat Transfer at Supercritical Pressures – Literature Review and Application to an HPLWR."

6. Davidson, Lars. "An Introduction to Turbulence Models." Chalmers University of Technology, Department of Thermo and Fluid Dynamics. Gotenberg, Sweden. November, 2003.
http://www.tfd.chalmers.se/~lada/postscript_files/kompendium_turb.pdf

7. Demboski, et al. "Evolutions in U.S. Navy Shipboard Sewage and Graywater Programs." 1997.

8. Freels, James D. "Application of FEMLAB on Supercritical Hydrogen Components of the High Flux Isotope Reactor Cold Source." Oak Ridge National Laboratory.

9. "Future Fuels." Naval Research Advisory Committee Report, April 2006.

10. Griffith, Peter, et al. "Deterioration in Heat Transfer to Fluids at Supercritical Pressure and High Heat Fluxes." Journal of Heat Transfer, Jan 1969.

11. "General Atomics: Hazardous Waste Destruction." General Atomics Corporate webpage, 14 Feb 2007. <http://demil.ga.com/haz/scwo.haz.html>

12. In, W.K., et al. "CFD Simulation of the turbulent flow and heat transfer in a bare rod bundle." Proceedings of ICAPP 2004, June 13 – 17, 2004, paper no. 4179.

13. Jones, W. P., et al. "The Prediction of Laminarization with a Two-equation Model of Turbulence." International Journal of Heat Mass Transfer. Volume 15, pp. 301 -314. 1972.

14. Hutto, Lara. "A Comprehensive Guide to Shipboard Waste Management Options." MTS/IEEE Conference and Exhibition, November 8, 2001.

15. Killea, William R., et al. “Supercritical Water Oxidation: Microgravity Solids Separation.” Society of Automotive Engineers, 1988.

16. Kim, Seong et al. “Numerical Simulation of the vertical upward flow of water in a heated tube at supercritical pressure.” Proceedings of ICAAP 2004, June 13 – 17, 2004, paper no. 4047.

17. Koshizuka, S., et al. "Numerical Analysis of Deterioration Phenomena in Heat Transfer to Supercritical Water." International Journal of Heat Mass Transfer. Volume 38, No. 16, pp. 3077 - 3084, 1995.

18. Koss, Larry. "Technology Development for Environmentally Sound Ships of the 21st Century: An International Perspective." Journal of Marine Science and Technology, 1997. Volume 1, pp 127 -137.

19. Kovenya, V. "On Some Approaches to Solve CFD Problems." Computers and Fluids, Volume 30, 2001. pp. 903 - 916.

20. Li, L. J., et al. "Turbulent Heat Transfer to Near-critical water in a heated curved pipe under the conditions of Mixed Convection." International Journal of Heat and Mass Transfer, Volume 42, pp. 3147 - 3158. 1999.

21. Majumdar, S. "Role of Under-relaxation in Momentum Interpolation For Calculation of Flow With Non-staggered Grids." Numerical Heat Transfer, Part A: Applicationss, 13:1, 125 - 132.

22. Markle, S.P., et al. "Enginering the Environmentally Sound Warship for the Twenty-First Century." Naval Engineer's Journal, May 1999. pp 189 - 217.

23. Marrone, Phillip, et al. “Salt Precipitation and Scale Control in Supercritical Water Oxidation – Part B: Commercial and Full-scale Applications.: Journal of Supercritical Fluids, 16 May 2003.

24. Murphy, Lawrence, et al. "Navy Shipboard Oily Wastewater Secondary Treatment: Evolution from Indentification of Need to Procurement of Ultrafiltration Membrane Systems Using Performance Specifications and Open Systems Architecture." Marine Environmental Engineering Technology Symposium, May 31 - Jun 1, 2001. Arlington, VA.

25. Newman, J.N. Marine Hydrodynamics. The MIT Press. Cambridge, MA. 1977

26. Oh, Chang H., et al. "Thermal-Hydraulic Modeling of Supercritical Water Oxidation of Ethanol.” Energy and Fuels, 1996. Volume 10, pages 326 – 332.

27. Peterson, A., Vontobel, P., Vogel, F., Tester, J. Manuscript in

preparation.

28. "PyroGenesis - Technologies - Plasma Arc Waste Destruction System." PyroGenesis corporate webpage. 14 Feb 2007. <http://www.pyrogenesis.com/content_en/technologies/pawds.asp>

29. Roelofs, F. "CFD Analyses of Heat Transfer to Supercritical Water Flowing Vertically Upward in a Tube." 1 December, 2004. Netherlands Ministry of Economic Affairs.

30. "Sewage Treatment." Marine Engineers Review, Nov 1998. pp 17 - 18.

31. Tang, Chun, et al. "Numerical Simulation of Steady Compressible Flows Using a Zonal Formulation. Part I: Inviscid Flows." Computers and Fluids, Volume 30, 2001. pp. 989 - 1001.

32. Tang, Chun, et al. "Numerical Simulation of Steady Compressible Flows Using a Zonal Forumulation. Part II: Viscous Flows." Computers and Fluids, Volume 30, 2001. pp. 1003 - 1016.

33. Tonn, Gina. Staron, Scott. Gutshall, Erik. "A Baseline Costing Model for Shipboard Waste Disposal." Marine Environmental Engineering Technology Symposium. May 31 - Jun 2001. Arlington, VA.

34. "Towards the Totally 'Green' Ship." Naval Architect, May 2002. pp. 14.

35. Wagner, et al. "The IAPWS Industrial Formulation 1997 for the Thermodynamic Properties of Water and Steam." Journal of Engineering for Gas Turbines and Power, January 2000, Vol. 122.

36. Yamagata, K. "Forced Convective Heat Transfer to Supercritical Water Flowing in Tubes." International Journal of Heat and Mass Transfer, Volume 15, pp. 2575 - 2593. 1972.

37. Yesodharan, Suguna. "Supercritical water oxidation: An environmentally safe method for the disposal of organic wastes." Current Science, volume 82, No. 9. 10 May 2002.

38. Data provided through the U.S. Navy's Worldwide Cost Reporting Analysis and Reporting Tool.

APPENDIX A SIMULATION RESULTS FOR SALSAN, 1000 ml/min, VARIOUS MESH SIZES

		KEHexA.out	Results			
	X	Y	Z	Distance	PeakRes	FinalResid
U-Mom_Separator	-0.005921	0	0.3758	0.34885	9.80E-04	2.05E-04
V-Mom-Separator	-0.002266	-0.00547	0.3938	0.366848	9.92E-04	2.08E-04
W-Mom-Separator	0.001832	0.000438	0.01523	0.01192	9.13E-04	7.62E-05
P-Mass-Separator	0.004243	-0.004243	0.015	0.013417	2.54E-06	5.54E-08
U-Mom-TubeIn	-0.000241	0	0.0045	0.022501	2.09E-05	1.77E-05
V-Mom-TubeIn	-0.000092	0.000222	0.0025	0.024501	2.05E-05	1.75E-05
W-Mom-TubeIn	0.000382	0.000076	0.002	0.025003	5.98E-04	7.48E-06
P-Mass-TubeIn	0	0.0004	0.019	0.00801	5.90E-08	4.23E-08
H-Energy-Separator	0.0004	0	0.402	0.375	1.28E-03	1.85E-04
H-Energy-TubeIn	0.000333	0.000222	0.027	0.0004	8.34E-03	3.67E-05
T-Energy-Needle	0.000156	-0.000785	0.015	0.012027	1.30E-03	1.01E-05
T-Energy-Titanium	-0.002828	0.005292	0.066	0.039459	1.50E-04	3.12E-06
K-TurbKE-Separator	0.0004	0	0.02775	0.00085	1.44E-03	2.50E-06
K-TurbKE-TubeIn	0.0004	0	0.02775	0.00085	3.86E-03	1.92E-06
E-Diss. K-Seperater	-0.00036	-0.000149	0.0005	0.026503	7.93E-04	2.19E-05
E-Diss. K-TubeIn	0	0.0004	0.027	0.0004	1.59E-03	2.51E-05
	Nodes	1172711				
	Elements	1401219				
		KEHexB.out	Results			
	X	Y	Z	Distance	PeakRes	FinalResid
U-Mom_Separator	0.005921	0	0.2348	0.207884	4.97E-03	2.34E-04
V-Mom-Separator	0	0.005921	0.3488	0.321854	2.92E-03	2.38E-04
W-Mom-Separator	0.001086	-0.000508	0.01508	0.01198	1.20E-02	8.38E-05
P-Mass-Separator	0.003276	0.004601	0.015	0.013263	9.86E-06	5.63E-08
U-Mom-TubeIn	-0.000001	0	0.0095	0.0175	6.90E-04	1.85E-05
V-Mom-TubeIn	-0.000084	0.000084	0.0035	0.0235	6.91E-04	1.79E-05
W-Mom-TubeIn	-0.000382	-0.000076	0.001	0.026003	4.46E-03	7.41E-06
P-Mass-TubeIn	-0.000283	-0.000283	0.027	0.0004	1.39E-06	4.25E-08
H-Energy-Separator	0	-0.0004	0.402	0.375	4.17E-03	2.37E-04
H-Energy-TubeIn	-0.000333	0.000222	0.027	0.0004	1.05E-02	4.38E-05
T-Energy-Needle	-0.000566	0.000566	0.0125	0.014522	7.82E-02	1.33E-05
T-Energy-Titanium	-0.003806	0.004638	0.064	0.037483	9.19E-03	7.35E-06
K-TurbKE-Separator	-0.001219	-0.002885	0.066	0.039126	6.50E-03	6.69E-06
K-TurbKE-TubeIn	-0.0004	0	0.027	0.0004	9.23E-03	1.30E-06
E-Diss. K-Seperater	0	0.00039	0.0015	0.025503	3.97E-02	2.30E-05
E-Diss. K-TubeIn	0.000283	-0.000283	0.002	0.025003	1.18E-01	2.44E-05
	Nodes	1521407				
	Elements	1761219				
		KEHexD.out	Results			
	X	Y	Z	Distance	PeakRes	FinalResid
U-Mom_Separator	-0.005666	-0.001719	0.162	0.13513	9.75E-04	1.97E-04
V-Mom-Separator	0	0.005921	0.126	0.099177	9.42E-04	1.99E-04
W-Mom-Separator	0	-0.005921	0.3578	0.330853	6.38E-04	6.66E-05
P-Mass-Separator	-0.004819	0.003574	0.017	0.011662	4.73E-07	5.66E-08

U-Mom-TubeIn	0.000206	-0.000085	0.0035	0.023501	2.09E-05	1.85E-05
V-Mom-TubeIn	0	0.000304	0.003	0.024002	2.05E-05	1.80E-05
W-Mom-TubeIn	0.000276	0.000276	0.002	0.025003	6.00E-04	7.48E-06
P-Mass-TubeIn	-0.000283	-0.000283	0	0.027003	5.91E-08	4.27E-08
H-Energy-Separator	-0.000283	-0.000283	0.402	0.375	1.31E-03	2.07E-04
H-Energy-TubeIn	0.000222	0.000333	0.027	0.0004	1.09E-02	2.02E-05
T-Energy-Needle	-0.000156	-0.000785	0.017	0.010032	1.29E-03	6.15E-06
T-Energy-Titanium	0.004243	0.004243	0.023	0.007212	9.37E-05	1.55E-06
K-TurbKE-Separator	0.000283	0.000283	0.02775	0.00085	1.08E-03	1.81E-06
K-TurbKE-TubeIn	0.000283	0.000283	0.02775	0.00085	2.47E-03	1.41E-06
E-Diss. K-Seperater	-0.000382	0.000076	0.0265	0.000634	1.03E-03	2.32E-05
E-Diss. K-TubeIn	-0.000153	-0.00037	0.027	0.0004	1.76E-03	2.47E-05
	Nodes	1617599				
	Elements	1869219				
		KEHexE.out	Results			
	X	Y	Z	Distance	PeakRes	FinalResid
U-Mom_Separator	0.001413	0	0.015	0.012083	2.84E-04	1.37E-04
V-Mom-Separator	0.001644	0.00397	0.402	0.375025	2.87E-04	1.39E-04
W-Mom-Separator	0.001526	0.000845	0.01523	0.011899	4.83E-04	3.86E-05
P-Mass-Separator	-0.000153	-0.00037	0.027	0.0004	5.71E-07	2.53E-07
U-Mom-TubeIn	-0.000092	0.000021	0.027	0.000095	2.23E-05	2.00E-05
V-Mom-TubeIn	0.000019	-0.000024	0.027	0.00003	2.19E-05	1.95E-05
W-Mom-TubeIn	0.000217	0.000324	0.027	0.00039	6.03E-04	8.57E-05
P-Mass-TubeIn	-0.000047	0.000026	0.027	0.000054	3.69E-07	2.11E-07
H-Energy-Separator	0.000222	0.000333	0.402	0.375	8.37E-04	1.05E-04
H-Energy-TubeIn	-0.000078	-0.000392	0.027	0.0004	1.21E-02	1.30E-03
T-Energy-Needle	0.000153	0.00037	0.027	0.0004	1.27E-03	1.17E-05
T-Energy-Titanium	-0.005971	-0.000588	0.064	0.037483	1.34E-04	1.19E-05
K-TurbKE-Separator	-0.000222	0.000333	0.027	0.0004	7.73E-04	1.11E-05
K-TurbKE-TubeIn	-0.000222	0.000333	0.027	0.0004	1.87E-03	4.39E-05
E-Diss. K-Seperater	0.000222	0.000333	0.027	0.0004	1.69E-03	1.04E-04
E-Diss. K-TubeIn	0.000078	0.000392	0.027	0.0004	3.07E-03	1.56E-04
	Nodes	2467559				
	Elements	2717469				

APPENDIX B - Cost Estimator Input, Output, and Calculation pages

Title	Value	Notes
Annual liquid waste disposal cost ($/gallon)	0	$/gallon
U/W Training Days	28	Number of U/W Training Days per Deployment Training Cycle; Will be automatically compressed when time between deployments drops below 12 months
Fleet Exercise U/W Days	21	Number of Fleet Exercise U/W Days per Deployment Training Cycle; Will be automatically depressed when time between deployments is less than 12 months
Foreign port Factor	0.0833333	Calculates Number of days ship spends in Foreign Ports per Deployment; Max number of days per any deployment is 25
Max Foregin Port visits	25	Variable that limits foreign port visits for longer deployments
Constant Non-homeport Visits	7	Constant number based on ammo onload/offload for each deployment; A variable number will be calculated based on time between deployments
Crew	364	Permanent ship's force
Attached Personnel	0	Attached crew (airwing, marines, battlegroup staff, etc)
Life Cycle	25	
Ship Class Size	24	
Construction Start Year		
Current Year		
Deployment Length A	6	
Deployment Length B	8	
Deployment Length C	9	

Cost Estimator - "Inputs"

Inputs:			Outputs Savings ($Million) 6/18	8/12	9/11	Mod Combination
Crew	364					
Life Cycle	25	Per Ship	3.25558	2.499807	2.465607	2.863683
#Ship Class	24	Per Class	78.13392	59.99538	59.17457	68.72839

Cost Estimator - "Snapshot Output"

# Training Days Per de	28									
Training decrement fac	0.6									
# Fleet Exercise Under	21									
Days in a year	365.25									
			Deploymer	6	6	6	8	8	8	9	9	9
ANNUAL VALUES			Length Bet	18	12	6	20.571	14.857	12	23.727	18.692	11
Underway			#Deployme	0.5	0.6667	1	0.42	0.525	0.6	0.3667	0.4333	0.6
		Individual Training		14	18.667	16.8	11.76	14.7	16.8	10.267	12.133	10.08
		Fleet Exercise		10.5	14	12.6	8.82	11.025	12.6	7.7	9.1	7.56
		Deployed		90	120	180	100.8	126	144	99	117	162
Inport												
	Homeport											
		POM		2047.5	2730	1638	1719.9	2149.9	2457	1501.5	1774.5	884.52
		Workday		31224	23924	16431	30906	25446	21418	32032	28288	23213
		Non-workday		6075.3	4654.9	3197	6013.3	4950.9	4167.3	6232.5	5504	4516.5
	Other than Homeport											
		Workday		3458	3882.7	4186	3166.8	3230.5	3494.4	3045.5	3069.7	3330.6
		Non-workday		873.6	1164.8	0	733.82	917.28	1048.3	640.64	757.12	0
	Foreign Port											
		Workday		351.87	351.87	351.87	351.87	351.87	351.87	351.87	351.87	351.87
		Non-workday		682.5	1213.3	2730	642.1	1003.3	1310.4	560.55	768.95	1474.2
	Total Person Hours per year			44828	38074	28743	43655	38201	34421	44472	40653	33950
	Total Gallons Per Year			1E+06	1E+06	948533	1E+06	1E+06	1E+06	1E+06	1E+06	1E+06
	Total Gallons Life Cycle			4E+07	3E+07	2E+07	4E+07	3E+07	3E+07	4E+07	3E+07	3E+07
	Total Cost Life Cycle in Millions			3.26	2.77	2.09	3.17	2.77	2.50	3.23	2.95	2.47
	Total Cost Ship Class			78.13	66.36	50.10	76.09	66.58	60.00	77.51	70.86	59.17

Cost Estimator - "Output All"

# Training Days Per deployment	28		# Fleet Exercise Underw	21						
Training decrement factor	0.6		Days in a year	365.25						
		Deploymer	6	6	6	8	8	8	9	9	9
ANNUAL VALUES		Length Bet	18	12	6	20.571	14.857	12	23.727	18.692	11
Underway		#Deployme	0.5	0.6667	1	0.42	0.525	0.6	0.3667	0.4333	0.6
	Individual Training		14	18.667	16.8	11.76	14.7	16.8	10.267	12.133	10.08
	Fleet Exercise		10.5	14	12.6	8.82	11.025	12.6	7.7	9.1	7.56
	Deployed		90	120	180	100.8	126	144	99	117	162
Inport											
Homeport											
	POM		20	26.667	16	16.8	21	24	14.667	17.333	8.64
	Workday		152.5	116.85	80.25	150.94	124.28	104.61	156.45	138.16	113.37
	Non-workday		61	46.738	32.1	60.378	49.711	41.843	62.579	55.264	45.349
Other than Homeport											
	Workday		9.5	10.667	11.5	8.7	8.875	9.6	8.3667	8.4333	9.15
	Non-workday		3	4	0	2.52	3.15	3.6	2.2	2.6	0
Foreign Port											
	Workday		1	1	1	1	1	1	1	1	1
	Non-workday		3.75	6.6667	15	3.528	5.5125	7.2	3.025	4.225	8.1

Deployment Optemp

#Deployed	Length De	6	8	9
0.25		91.3125		
0.333333		121.75		
0.5		182.625		

#Deployed	Length De	6	8	9
0.28			136.36	
0.35			170.45	
0.4			194.8	

#Deployed	Length De	6	8	9
0.275				150.6656
0.325				178.0594
0.45				246.5438

				365.25	365.25	365.25	365.25	365.25	365.25	365.25	365.25	365.25

Cost Estimator - "Optempo"

Total hours	24		
		Other than	Foreign
Homeport		Homeport	Port
Number Duty Sections	6	3	3
Normal Work Hours	0	0	0
Factor	0	0.7	0.5

Notes
Factor is meant to capture the fact that although it is a not workday, much of the crew will remain onboard or return after a night of liberty and produce liquid waste

Cost Estimator - "Non-Workday"

Total hours	24		
Homeport		Other than	Foreign Port
Number Duty Sections	6	3	3
Normal Work Hours	10	12	12
Factor	0	1	0.9

Notes
Factor is meant to capture the fact that although it is a not workday, much of the crew will remain onboard or return after a night of liberty and produce liquid waste

Cost Estimator - "Workday"

		Rate (gallons ppd)	Crew Size	Attached Crew	Person Hours						
Underway			0								
Inport					S/f	Duty Section	Person Hours Totals (hours)	Person Days Total (days)	GPPD		Gallons Liquid Waste / Day
Homeport		0.166667									
	POM		33	364	0	1729	728	2457	102.375	33	3378.375
	Workday					3458	1456	4914	204.75	33	6756.75
	Non-Workday					873.6	1516.7	2390.2667	99.59444	33	3286.617
Non-homeport		0.333333								33	
	Workday					5824	2912	8736	364	33	12012
	Non-Workday					4076.8	2912	6988.8	291.2	33	9609.6
Foreign Port		0.333333								33	
	Workday					5532.8	2912	8444.8	351.8667	33	11611.6
	Non-Workday					1456	2912	4368	182	33	6006

Cost Estimator - "Gallons Per Day"